WILDFIRE DETECTION SYSTEM BASED ON PRINCIPAL COMPONENT ANALYSIS AND IMAGE PROCESSING OF REMOTE-SENSED VIDEO

A Thesis

presented to

the Faculty of California Polytechnic State University,

San Luis Obispo

In Partial Fulfillment

of the Requirements for the Degree

Master of Science in Electrical Engineering

by

Ryan F. Radjabi

June 2016

COMMITTEE MEMBERSHIP

TITLE:	Wildfire Detection System Based on Principal Component Analysis and Image Processing of Remote-Sensed Video
AUTHOR:	Ryan F. Radjabi
DATE SUBMITTED:	June 2016
COMMITTEE CHAIR:	John Saghri, Ph.D. Professor of Electrical Engineering
COMMITTEE MEMBER:	John Jacobs, Ph.D. Raytheon Professor of Practice
COMMITTEE MEMBER:	Jane Zhang, Ph.D. Professor of Electrical Engineering

ABSTRACT

Wildfire Detection System Based on Principal Component Analysis and Image Processing of Remote-Sensed Video

Ryan F. Radjabi

Early detection and mitigation of wildfires can reduce devastating property damage, firefighting costs, pollution, and loss of life. This thesis proposes the method of Principal Component Analysis (PCA) of images in the temporal domain to identify a smoke plume in wildfires. Temporal PCA is an effective motion detector, and spatial filtering of the output Principal Component images can segment the smoke plume region.

The effective use of other image processing techniques to identify smoke plumes and heat plumes are compared. The best attributes of smoke plume detectors and heat plume detectors are evaluated for combination in an improved wildfire detection system. PCA of visible blue images at an image sampling rate of 2 seconds per image effectively exploits a smoke plume signal. PCA of infrared images is the fundamental technique for exploiting a heat plume signal. A system architecture is proposed for the implementation of image processing techniques. The real-world deployment and usability are described for this system.

Keywords: Image Processing, Principal Component Analysis (PCA), Infrared, Spatial Filtering, Segmentation, Wildfire, Forest Fire

ACKNOWLEDGMENTS

I would like to thank Dr. Saghri and Dr. Jacobs for proposing this noble and exciting project. I would like to thank them for their commitment and patience with my thesis. I'd also like to thank Raytheon for their sponsorship of the EFFD project and the Goleta fire experiments. I'd like to thank my friend Dennis for continuously asking, "How goes your thesis?"

Lastly, I would like to thank my family for their love, encouragement, support, and patience. Thank you Mom and Dad for caring so deeply that I finish my research. Thank you Emily for your love, your care, and your support.

TABLE OF CONTENTS

LIST OF FIGURES

Page

1 INTRODUCTION

1.1 Background and Motivation

Early detection and mitigation of wildfires should be desirable for public agencies such as fire departments, state/national parks, and state governments. On the order of $2 billion is spent each year by the United States [1] to fight wildfires. In addition, the costs of lives and personal property are devastating to families and individuals. Forest fires are estimated to contribute 20-30% of global carbon emissions each year [2]. Research and development to create a modular and intelligent early fire surveillance and detection system should be a priority for environmental organizations.

1.2 Existing Fire Detection Technology

Fire detection systems exist in real-world application with varying technology and maturity. On the most mature side are industrial and manufacturing applications of fire detection, and on the less mature side are the applications toward wildfire detection.

1.2.1 Industrial and Manufacturing Fire Detection

Close range fire detection has been developed for factory safety procedures. It is commonly used to thermally sense aberrations in manufacturing processes in order to trigger mitigation measures. The field of view is small and uses high resolution (thus a small footprint) due to the proximity of the imaging element.

1.2.2 Land-Based Wildfire Detection

Visible spectrum surveillance has been attempted in many settings. The common method is to detect smoke in a large field of view with stationary (and sometimes with zooming)

cameras. These are susceptible to false triggers for the following reasons: 1) smoke is often imperceptible from environmental features like fog and clouds, 2) background smoke can easily be confused with foreground noise such as dust and moisture on the imaging lens. A high rate of false triggers usually means the system will require frequent human interaction to verify triggers.

Insight Robotics is a Hong Kong startup that has developed a land-based system for detecting wildfires [2]. The Insight Robotics system consists of a thermal imaging camera, a fog-penetrating visible camera, and an on-board processor.

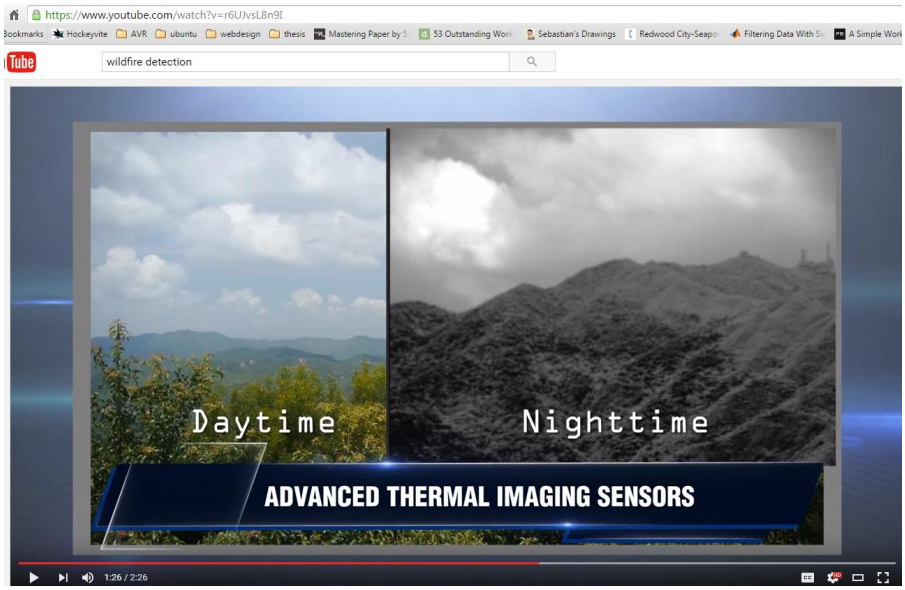

Figure 1 - Insight Robotics Visible and Thermal Imaging System for Fire Detection.

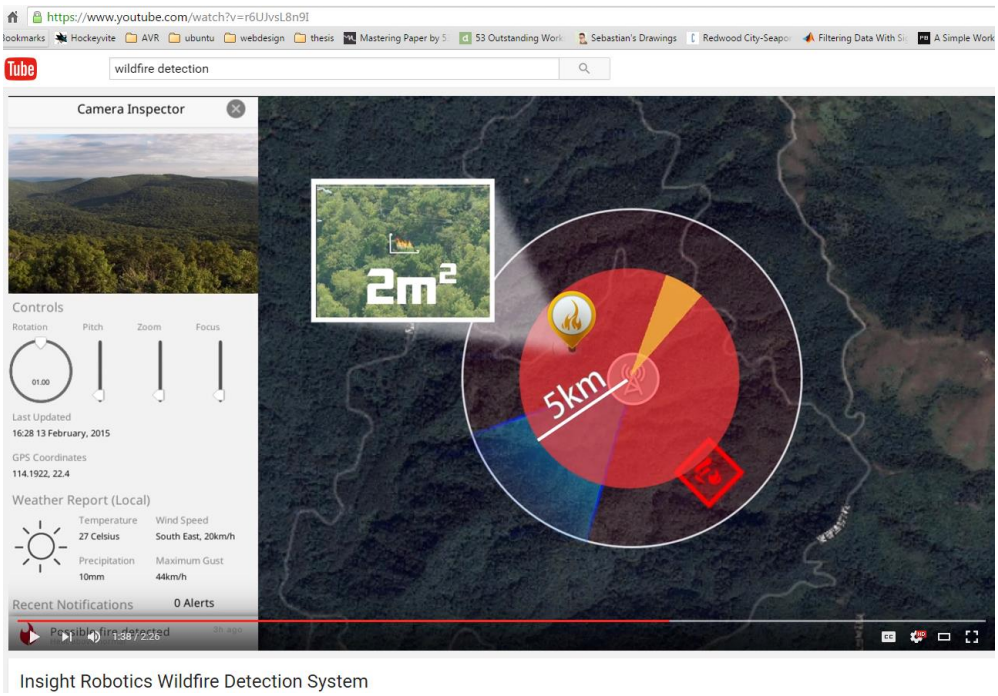

Figure 2 - Insight Robotics Fire Detection Showing Fire Location.

A number of wildfire detection systems have been designed to detect and track known fires. This application is useful for firefighting crews to assess the coverage of a fire and anticipate its spread. It is important to recognize the distinction between a system that detects the conception of a fire and a system that tracks a known fire.

1.2.3 Aerial Wildfire Detection

Aerial surveillance is effective for reactively monitoring wildfires. Once a wildfire is detected, aircrafts can be used to track the movement of a wildfire. Manned aircrafts are expensive to fly 24/7, as would be necessary for an early-detection system. Satellites can also track wildfires, but the footprint of satellite cameras is too large to detect wildfire conception. Once again, this method is better suited for tracking progress of fires. The drawbacks with the satellite forest fire detection systems are twofold: 1) inability to perform 24/7 surveillance of the

same geographical area, and 2) inadequate spatial resolution (footprint) for early forest fire detection.

1.3 History of Early Forest Fire Detection Research at Cal Poly

EFFD was first described by Drs. John Jacobs and John Saghri in 2009 as a problem statement: Forest fires are devastating, and their seasonal occurrence is inevitable. While preventing forest fires is unrealistic, it is possible to improve the detection of fires and decrease the response time for firefighters. A land-based monitoring system could be designed using image processing techniques to improve wildfire detection.

This project began in 2009 by MSEE student, Ryan Radjabi, and BSEE students, Bryce Du, Dennis Keyes, and John Cape. The first year of the project was exploratory in an attempt to characterize the behavior of infrared imaging around various heat sources. Backyard experiments with paper, firewood, gas grills, charcoal grills, and foliage were attempted <<insert backyard and frontyard imaging, observed from close range as well as long range at the football field>>. One experiment was done using the FLIR uncooled, LWIR camera from the parking lot around Student Housing North during a Cal Poly Open House viewing club barbecues. Night-time bonfires were also viewed in Avila beach using the FLIR Merlin infrared camera connected to a PC with a National Instruments frame-grabber, powered by a car battery. These were the early attempts at data collection where some of the following challenges were discovered: synchronization of fire and recording, data acquisition, data storage capability, ensuring ample battery and AC power supplies.

In the summer of 2010, a group of students participated in a study at Raytheon's Goleta facility as the most serious experiment to date. With the assistance of Raytheon engineers, the team recorded fires caused by various fuels from a video recording tower about one kilometer

from the source barbecue. This day-long experiment became the source data for the 2011 SPIE paper. Much like the less-organized data collection ventures in backyards, at Open House barbecues, and at Avila beach, the same challenges arose in the coordinated experiment. The team experienced issues synchronizing DAQ systems (LWIR & MWIR & visible), and managing massive amounts of data with limited storage capacity (i.e., a 1024x1024 video recording on a 14-bit frame-grabber at 2 Bytes per pixel and 30 frames per second consumes 60 MB per second or 3.6 GB per minute). Note-taking became an issue while attempting to recall the sequence of events throughout the day, which was necessary for correlating data sets with fuel type.

1.4 Structure of this Paper

This paper is a survey of the efforts in EFFD at Cal Poly from 2009 until 2015. In 2011, the novel method of temporal PCA of IR images was presented at SPIE, based on data collected in the 2010 Goleta Fire Experiment. Since then, six students have completed their Masters theses on the subject: Moussa (2012), Kohler (2012), Davenport (2012), Boynton (2013), Aldama (2013), and Garges (2015). Papers have been published at SPIE Optics and Photonics, Applications of Digital Image Processing Conference in 2011, 2012, and 2015 based on the thesis work of those students.

Chapter two describes the first proposed EFFD technique (Temporal PCA of IR Images) by Ryan Radjabi in the 2011 SPIE paper. Chapter three is a review of the thesis work on EFFD from the other MSEE students on the project from 2012-2015. Chapter four is a comparison of the most successful methods, followed by a proposed combination of the most successful methods, and the comprehensive design of an EFFD system. Chapter five is a conclusion and suggests some open areas of research in the proposed implementation.

2 PROPOSED TECHNIQUE

2.1 Description of PCA

A novel technique is described that senses subtle variations in infrared radiation from a natural scene. It uses a land-based camera to observe a fixed position and constantly monitors for temperature variations using Principal Component Analysis (PCA). PCA, in short, is a mathematical procedure that converts a set of possibly correlated variables into a set of values of linearly uncorrelated variables called principal components. Applying PCA to a temporally related set of images creates the effect of re-mapping the image set into new images that are ranked by their strength of eigenvectors. If four input images are used of the same scene containing a boulder, a large tree, and an animal running across the view, the following output images can be expected. In decreasing order of "principal value":

1) The boulder would be prominent and appear in every input image because it is static, so it would be the most weighted feature and certainly appear in PC1.
2) The large tree is less static than the boulder because it will sway in the wind, but its trunk is mostly stationary, so it would appear prominent in PC2.
3) The leaves of a tree and its canopy will sway in the wind and have a fair amount of variability relative to the previous objects, so it would appear in PC3.
4) Lastly, the animal that runs across the scene is never in the same location in any frame, so it would appear as a streak across the image in PC4. PC4 is the least common dataset of the four input images and anomalies will manifest themselves in this image.

Much like an animal running across the previously described scene, PCA will detect anomalous fluctuations in temperature caused by a newly forming fire (to an infrared camera). Temperature fluctuations of the fire and new formations of smoke will disrupt the scene only slightly, and that is what is most noticeable in lower principal components, the slight, subtle variations.

2.2 Temporal PCA as Reported in 2011 SPIE Paper

The 2011 SPIE paper, titled "Early Forest Fire Detection Using Principal Component Analysis of Infrared Video," presented the technique of temporal PCA of IR video in order to detect a fire plume [3]. The data set was based on the initial Goleta fire experiment in 2010. A set of cameras, including visible RGB, LWIR, and MWIR, were mounted on a 20-meter tall tower to record multispectral video of the fire scene. This paper presents the results of initial experimentation using 8-bit LWIR data. It should be noted that analysis in 2011 SPIE was only using IR camera, thus it was able to detect the fire core and surrounding heat. At the time, it wasn't clear whether or not a "heat plume" could be detected in IR. It was later determined that the IR detector is too insensitive to capture a heat plume, or there is not considerable thermal variation at such a distance [4].

PCA was applied on a series of images collected in the 2010 Goleta experiment. The initial hope was to collect visible spectrum, LWIR, and MWIR images from a similar vantage point, and perform multi-spectral PCA on a scene. This however did not produce the results expected. Some notable challenges were temporal and spatial registration.

It was discovered that temporal PCA from the LWIR spectrum created prominent signals in lower principal component images. Testing a range of sampling frequency (temporal spacing)

had a very noticeable impact. Temporally-spaced PCA of LWIR proved to gather the largest signature of the fire plume.

The temporal signatures within the fire plume area exhibited temporal and spatial randomness. The randomness of this region does not statistically influence the covariance matrix whose eigenvectors form the PCT matrix. A majority of the FOV consists of stationary features that dominate the covariance matrix[i]. The proposed method was PCA of 10 8-bit LWIR images spaced at 1s. PC 7 of a 10 frame PCT exhibits the most visible signature in the fire plume region. After median filtering and thresholding, segmentation of the fire plume was achieved. The superiority of PCT against simple frame differencing is shown in Figure 3, Figure 4, Figure 5, and Figure 6.

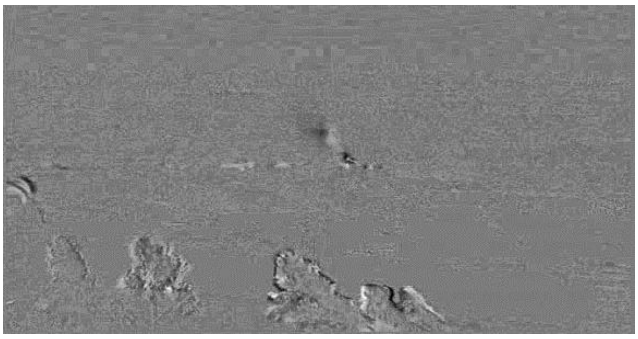

Figure 3 - The 7th PC image showing the traces of the fire plume and moving tree branches against a mostly flat background. Source: SPIE 2011

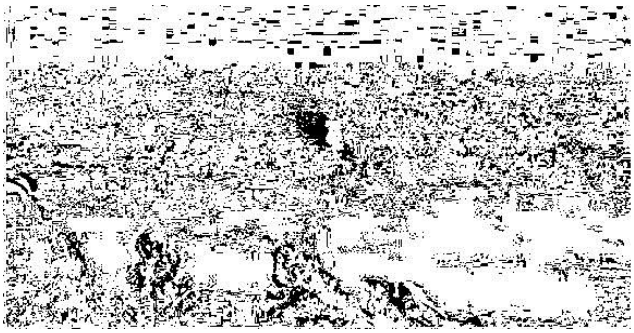

Figure 4 - Result of applying simple threshold operation (Threshold = 110) to the 7th PC image in Figure 3. Source: SPIE 2011

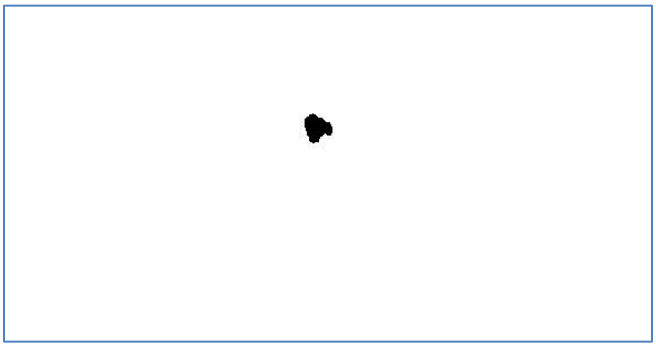

Figure 5 - Final result after applying a median filter of kernel size 21 to the threshoded 7th PC image shown in Figure 4. The fire plume appears as an isolated black spot. Source: SPIE 2011

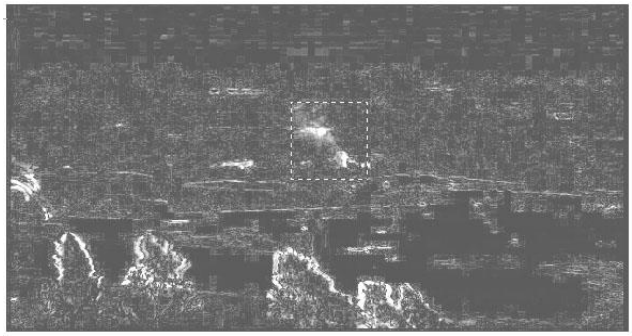

Figure 6 - Result of change detection via simple differencing. The image shown is formed by adding up the difference images between each consecutive pair of frames within the 10s capture period. Source: SPIE 2011

The 2011 SPIE scheme set the foundation for follow-up research in EFFD by other students. These schemes will be discussed in further detail in Chapter three. Temporal PCA of a

chosen spectral band was challenged and improved upon using data collected from the 2011 Goleta fire experiment. Ultimately, single-band temporal PCA was found to be the most effective method and the simplest method.

3 REVIEW OF EFFD RESEARCH AT CAL POLY

3.1 Moussa

3.1.1 Summary

Georges Moussa's thesis [4] studies fire core detection and smoke plume detection. Fire core detection is attempted with range filtering and entropy filtering of IR video data. Range filtering and entropy filtering techniques did not successfully segment fire core, and will not be discussed to greater detail. Smoke plume detection is achieved by performing PCA on visible spectrum video data followed by motion analysis and adaptive intensity thresholding. PCA and adaptive intensity thresholding on visible blue images was demonstrated as an effective smoke plume detection with low false-alarm rates. This method will be described later in this paper.

3.1.2 Review

Moussa explores techniques for detecting the fire core and the smoke plume. Fire core detection is first explored with an examination of texture analysis filters. Texture analysis filters are effective at segmenting regions when intensity thresholding is less effective. Four distinct texture analysis filters were examined: Range Filter, Standard Deviation Filter, Entropy Filter, and Absolute Difference Filter. Range filtering replaces the center pixel value with the difference of the kernel maximum and minimum. It reveals edges and texture of the image. Standard Deviation filtering replaces the center pixel with the local standard deviation of the kernel. It highlights edges and areas with high intensity changes. Entropy filtering produces a binary image based on a determined measure of intensity randomness which characterizes texture of the neighborhood pixels. Absolute Difference filtering creates a difference image from consecutive frames. The best results from texture analysis were achieved by combining filters. The sequence

of Range Filter of two consecutive frames, absolute difference of the two output frames, followed by entropy filtering segmented the fire core. Its strength was its ability to segment the fire core without any thresholding or parameter tuning. It also succeeded in suppressing noise and moving objects.

The author experimented with PCA of the visible spectrum to segment smoke plume. PCA has been previously identified as a successful change detector and the PC2 & PC3 images capture the growing smoke plume due to its unique temporal variation. The superiority of PCA versus Absolute Difference filtering is demonstrated in Figure 7 below.

Figure 7 – Original Visible Frame, Absolute Difference of Two Consecutive Visible Frames, Scaled PC2 of Blue Band, from Left to Right, Respectively. Source: Moussa Figure 26

Next, the author explores techniques for segmenting the smoke plume from PC2. The Gaussian Mixture Model technique tests each pixel against a probability distribution to score it as a background or foreground pixel. This method is demonstrated in Figure 8 below. It was strongest at segmenting a large and moving smoke plume, but its weakness was in capturing small plumes and stationary plumes.

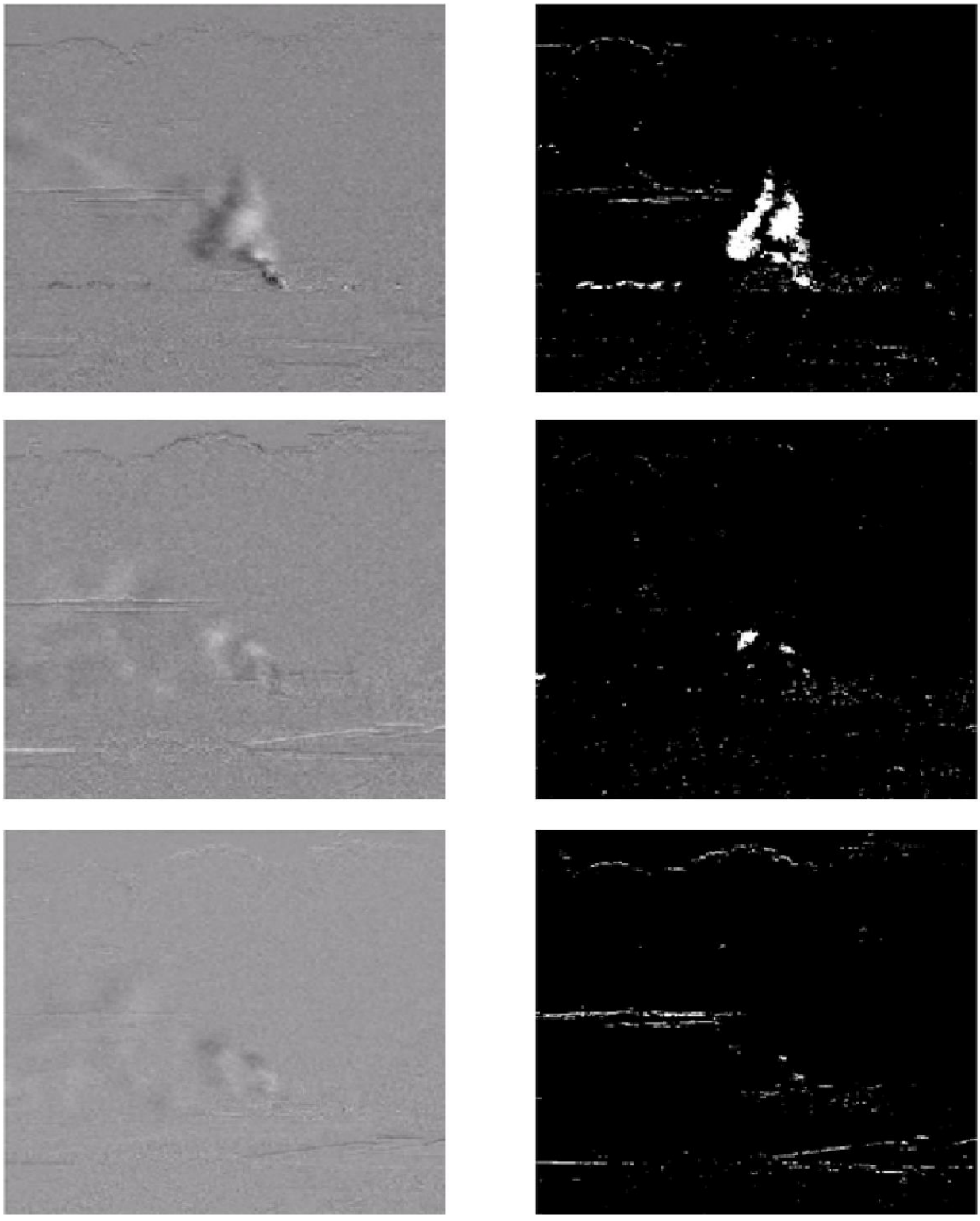

Figure 8 - PC2 compared with GMM Results. Temporal Blue Band PC2 frames on Left, Binary images after GMM on Right. Source: Moussa Figures 31-35

Due to the intensity variations of PC images, the same intensity threshold for one image cannot be applied to the next in the sequence and properly segment the plume. An algorithm was written to adaptively adjust the threshold over a sequence of frames. This method is called Adaptive Intensity Thresholding and it is calculated by placing a threshold window centered on the highest histogram count computed in the image. The instantaneous total segmented area per frame is measured and plotted for a video sequence. Smoothing was applied with a 20 frame moving average to the curve. The results are displayed in Figure 9 using ~450 frames. The curve indicates a peak around frame 175 that indicates the peak smoke plume instance.

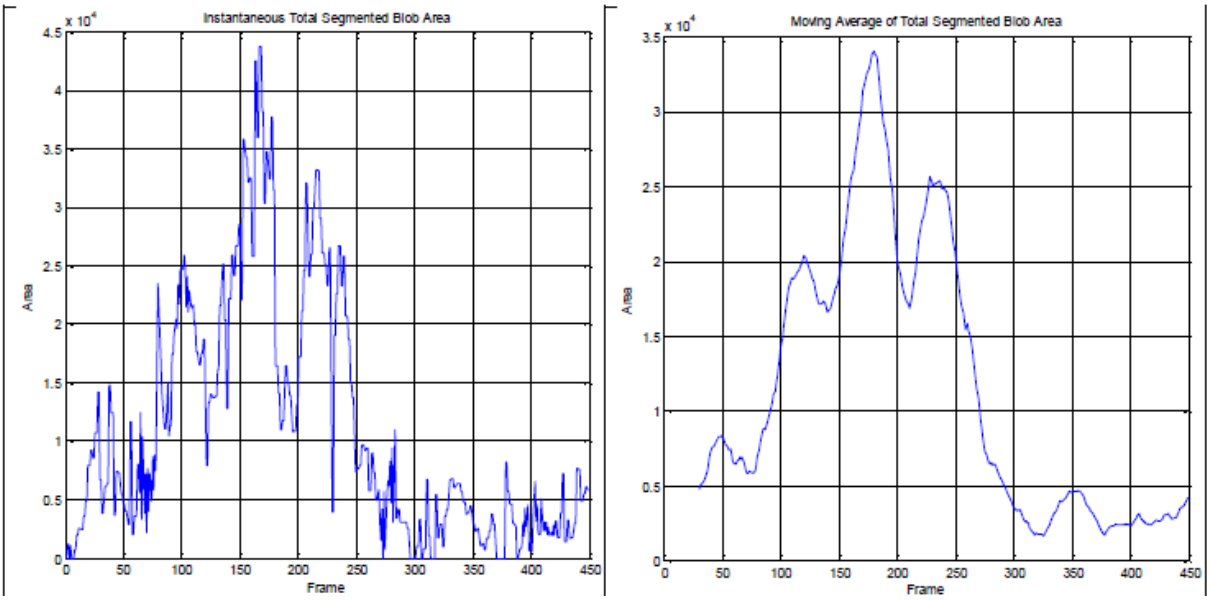

Figure 9 - Results of Adaptive Intensity Thresholding. On the Left, Instantaneous Total Segmented Area per frame using Adaptive Threshold Technique; On the Right, 20 Frames Moving Average of Total Segmented Area per Frame using Adaptive Threshold Technique. Source: Moussa Figure 46

The author makes an observation in Chapter 7 that the histograms of PC2 are dramatically different. In particular, the background intensity value changes between consecutive PC2 images, see Figure 10. The theory is that dynamic range adjustment from the 0-centered values output from PCA to the 8-bit scaled values causes significant background intensity

variations. The proposed solution is to calculate the absolute change by taking the absolute value of all PC2 pixels before mapping to 8-bit for display. The same temporal PCA procedure is applied except the absolute value of the PC images is calculated before scaling to the full dynamic range.

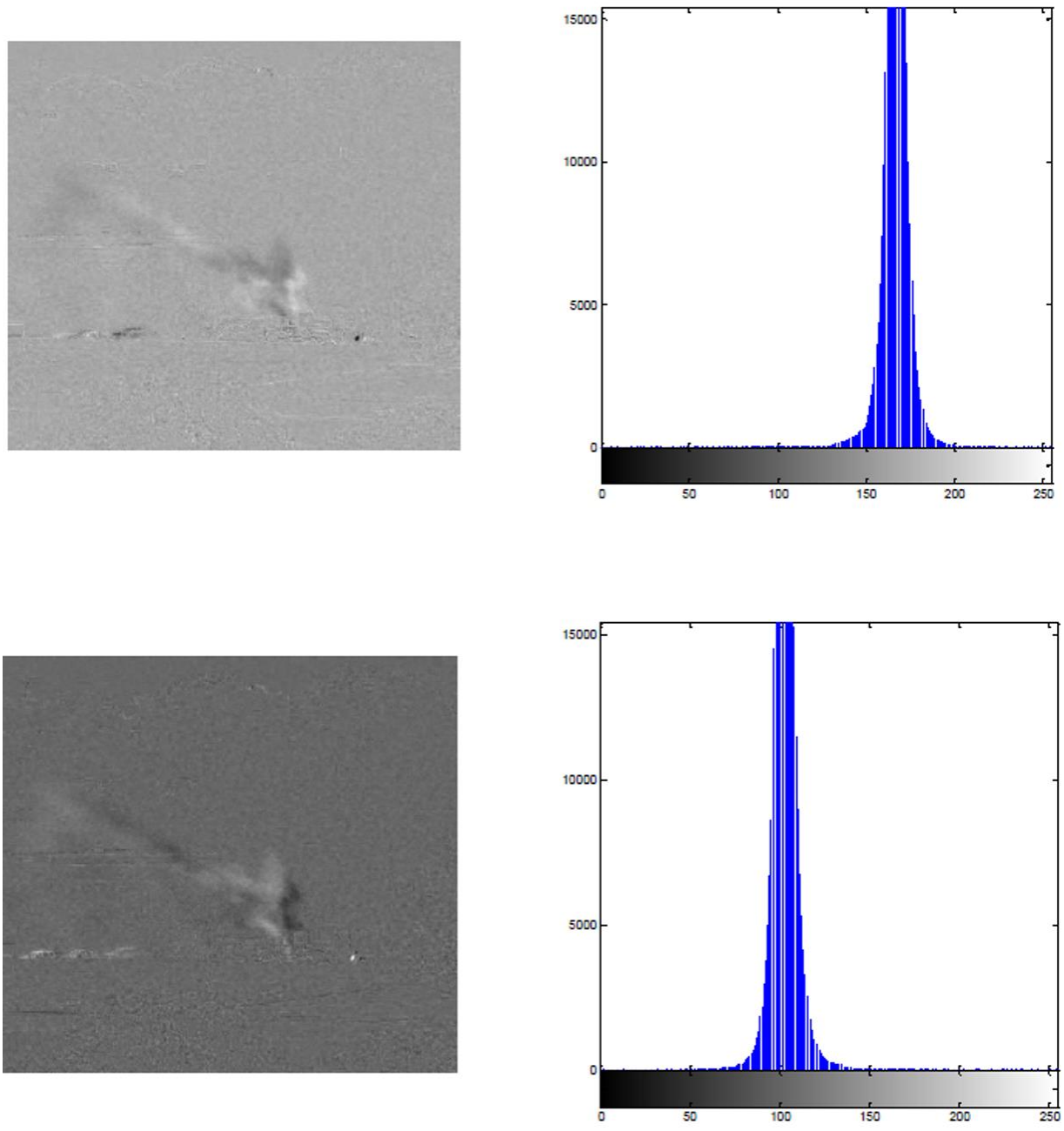

Figure 10 - Evidence of Background Intensity Changes for Consecutive PC2 Images. PC2 Frame 7890 of "Oats1" on Left, and histogram on Right. Source: Moussa Figures 47,48

Finally, the author experimented with spectral PCA using three time instances and RGB bands. The PCA input was still nine images, but a different period and sampling interval. The

true effect was spectral-temporal PCA, and the results did not appear to be any better than Blue band analysis. The best smoke plume signal is found in PC4 and PC5.

The author ultimately designed the smoke plume detection system as a combination of temporal blue band PCA and included pre-processing and post-processing steps that were experimented throughout the paper. The deeper discussion of this method is described in Chapter 4 of this paper.

3.1.3 Suggestions

Moussa identifies visible blue as the best spectrum for temporal PCA to exploit a smoke plume. The method would benefit from advanced pre- and post-processing techniques. Papers by Kohler, Davenport, Boynton, and Aldama experiment with pre- and post-processing filters that successfully reject noise and maintain signal strength. Garges expands upon Moussa's PCA of visible blue by picking the optimal sampling rate and the PCA input size.

3.2 Kohler

3.2.1 Summary

Daniel Kohler's thesis [5] researches heat plume detection from cooled MWIR video. Variance Set Statistics analysis was performed to explore its ability to segment heat plume. Statistical analysis alone was not a conclusive heat plume detector, but it provided insight in ways of classifying heat plumes. Principal Component Analysis was performed on the results of Variance Set Statistics filters with great results. The success and utility of PCA-DRMAD for heat plume detection will be discussed in greater detail in Chapter 4 of this paper. Lastly, a Support Vector Machine (SVM) was designed in an attempt to use machine learning to train and

produce a heat plume detection algorithm. The SVM was not successful in classifying heat plumes from IR images.

3.2.2 Review

Kohler identified a set of "features" which themselves are analysis techniques. Variance, Variance Set Statistics, Simple Moving Average (SMA), Exponentially Weighted Moving Average (EWMA), Dual-Range Moving Average Difference (DRMAD), and PCA were the described features. Variance was chosen as a feature because it over time represents information about movement, and movement is a characteristic of heat plumes. The heat plume should have a unique variance compared to other objects as demonstrated in Figure 11.

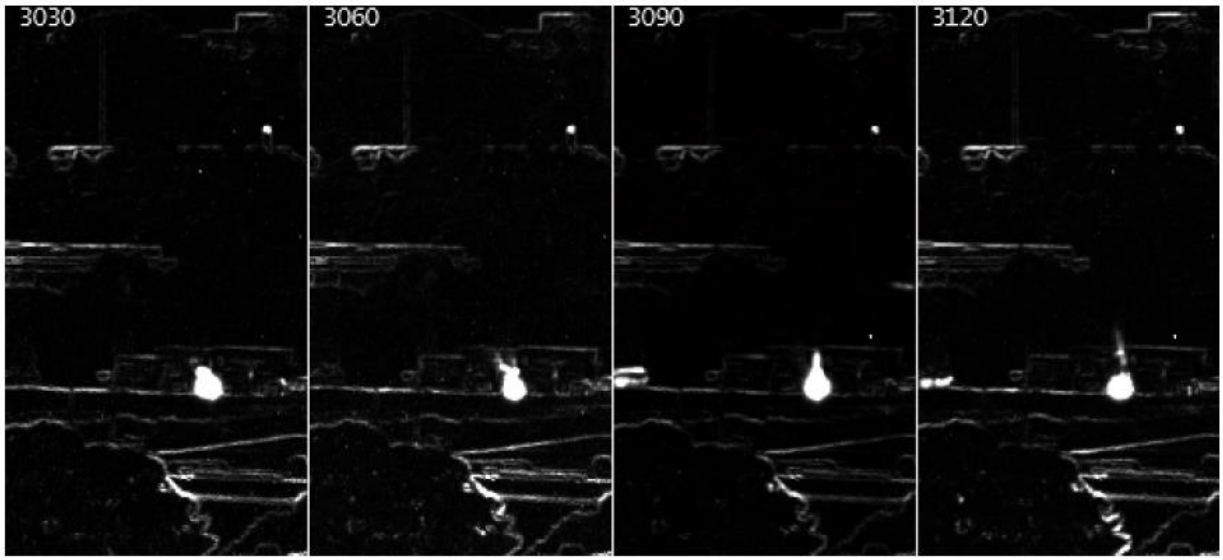

Figure 11 - 30 Frame Pixel-wise Variance Calculation Showing a Prominent Heat Plume. Source: Kohler Figure 16

Variance Set Statistics are the set of minimum, maximum, mean, and median calculations. These were examined in various regions of interest (ROIs) identified in the scene. An analysis is made on the pixel means comparing three ROIs, grassy field, foreground foliage, and heat plume. Evidence of this analysis is shown in Figure 12.

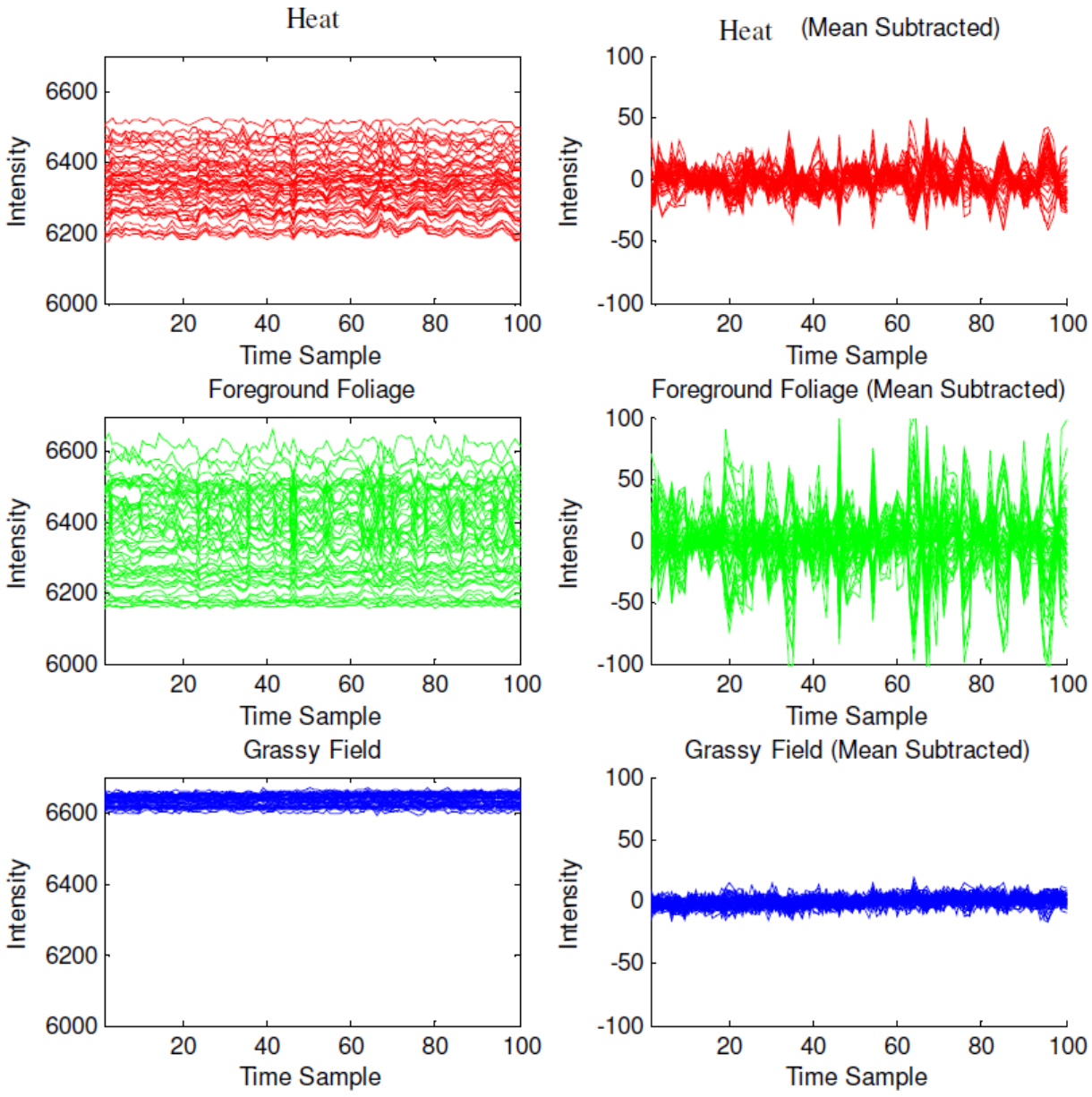

Figure 12 - Pixel Means of ROIs. Source: Kohler Figure 19

EWMA is a modification of SMA that weighs recent frames more heavily than older frames in averaging. DRMAD is a modification of EWMA that is a difference of EWMAs such that DRMAD = EWMA_short – EWMA_long. This is an effective filter to remove noise, as demonstrated in Figure 13.

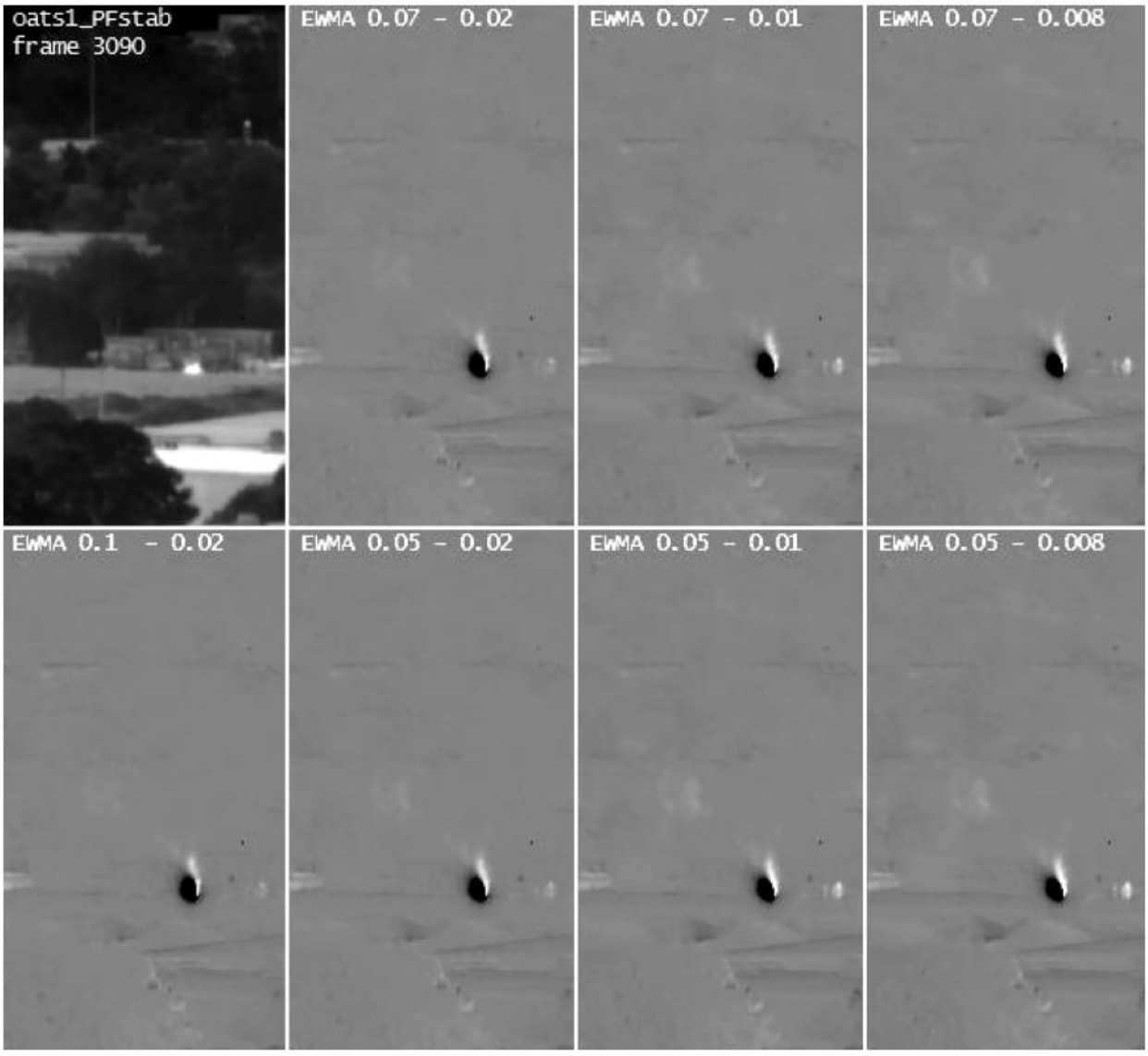

Figure 13 - DRMAD pairs with varying p-values. Source: Kohler Figure 22

Chapter 5 of Kohler's paper combines previously identified "features" in order to segment the heat plume and produce a binary image. Some methods produced poor results such as the Variance Corridor Classifier, and the Mean and Max Thresholding (MMT) classifier. The Variance Corridor classifier based solely on variance detected motion indiscriminately, and passed far more than just the heat plume. The MMT classifier did not effectively differentiate

between heat plume and noise plus moving objects. The best results were achieved after subtracting a length 10 filter, and then median filtering with at 5x5 kernel.

The following two methods produced successful results. Mean by Median (MBM) had better results than the previous methods. When intersected with the variance threshold, intermittent objects were filtered out, though it still had false positives from pedestrians and vehicles. PCA-DRMAD shows promise as a filter that improves heat signal over background noise. PC1 serves as a measure of persistence, which is a primary attribute of the heat plume. PCA-DRMAD filters out every leading challenge category in PC1, and only detects 43 non-heat pixels through a range of video (frames 510-5000), while retaining the heat plume signal, see results in Figure 14.

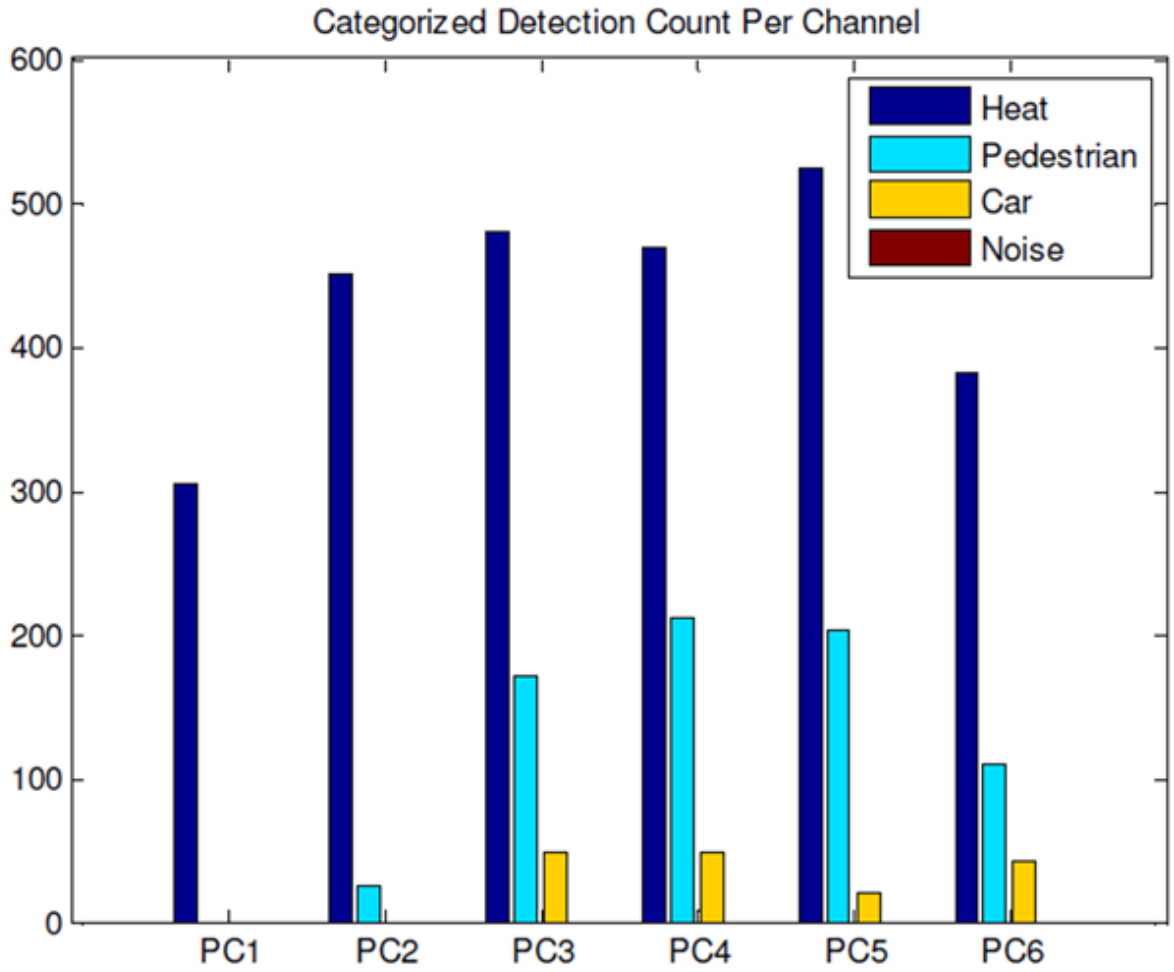

CDC Comparing Auto-Thresholded PC Images
(Difference Case 1)

Error Analysis for PCA-DRMAD
(Difference Case 1)

Channel name:	Heat	Not	E_avg
EWMA0.07-0.02_PCA6_autolinear_auto-th\1	304	43	0.026
EWMA0.07-0.02_PCA6_autolinear_auto-th\2	450	116	0.071
EWMA0.07-0.02_PCA6_autolinear_auto-th\3	479	197	0.070
EWMA0.07-0.02_PCA6_autolinear_auto-th\4	469	231	0.069
EWMA0.07-0.02_PCA6_autolinear_auto-th\5	523	217	0.099
EWMA0.07-0.02_PCA6_autolinear_auto-th\6	382	144	0.057

Figure 14 - Low False Positives in PC1 from PCA-DRMAD. Source: Kohler Figure 41 and Table 22

Principal Image Combination takes the results of PCA-DRMAD and adjusts the classifier to be a heat plume pixel if it is a member of the dilated PC1 image (using a radius 3 dilation) and at least one other PC image. The results in Figure 15 show low error rates in the Principal Image Combination classifier.

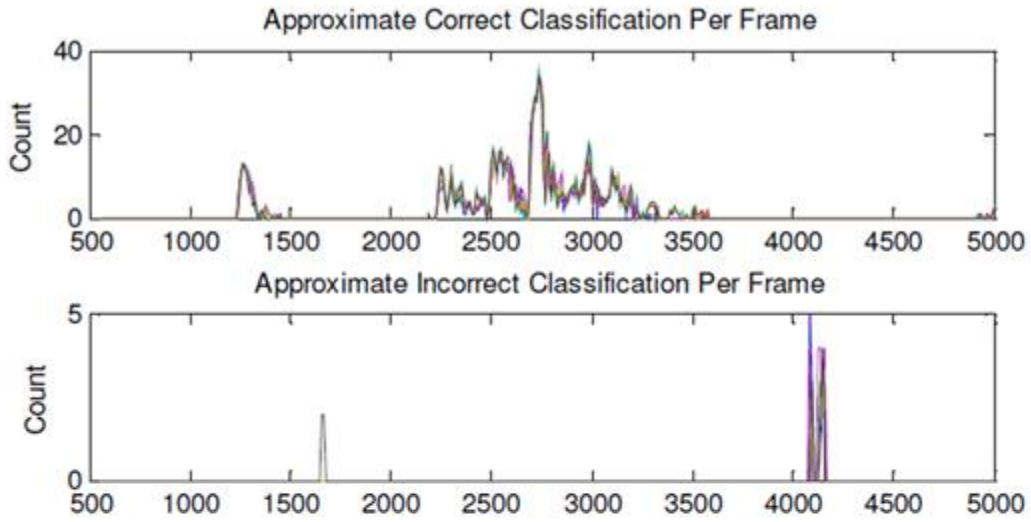

Comparison of Classifiers for All PCA-DRMAD Difference Configurations

Error Analysis for All PCA-DRMAD Difference Configurations

Case	Channel name:	Heat	Not	E_avg
1	EWMA0.1-0.02_PCA6_autolinear_auto-th_c1	871	15	0.013
2	EWMA0.07-0.02_PCA6_autolinear_auto-th_c1	931	17	0.016
3	EWMA0.07-0.01_PCA6_autolinear_auto-th_c1	918	11	0.011
4	EWMA0.07-0.008_PCA6_autolinear_auto-th_c1	944	10	0.009
5	EWMA0.05-0.02_PCA6_autolinear_auto-th_c1	950	23	0.013
6	EWMA0.05-0.01_PCA6_autolinear_auto-th_c1	937	9	0.009
7	EWMA0.05-0.008_PCA6_autolinear_auto-th_c1	928	15	0.013

Figure 15 - Principal Image Combination. Source: Kohler Figure 43, Table 23

The author next experimented with heat plume detection using a Support Vector Machine (SVM). A SVM trains from a set of observations belonging to a known binary class, then it classifies new observations based upon its trained state [21 from Kohler]. This SVM uses a Radial Basis Function kernel. Positive training data was taken from pixels in the heat mask region and negative training data was taken from pixels outside the heat mask. The author chose two sets of signals for SVM training data. The first set was the Principal Component of each pixel. Each pixel's data set was a vector of its Principal Component weights. The second set was the PC images – PC1, PC2, and PC3 were used from two time instances. The SVM was unable to learn distinctions between heat and non-heat points. The author provided the following reasons to failure: 1) training error 2) failure masking the heat region 3) mismatching sampling interval for training data and input data. The inconclusive results of the classification output applied to PC6 are displayed in Figure 16.

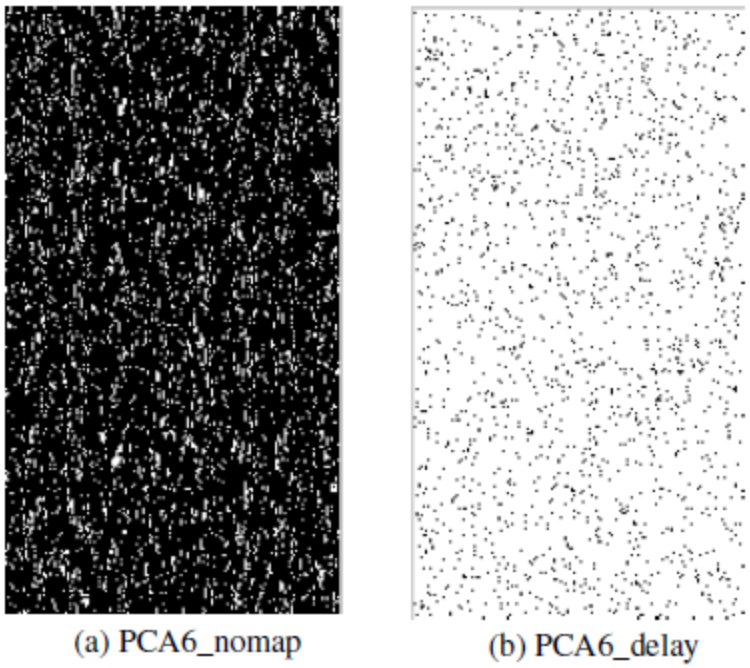

Figure 16 – Support Vector Machine Output. Source: Kohler Figure 45

3.2.3 Suggestions

The results from VSS classification are promising, and the artifacts that exist in Figure 11 could be filtered out using some general assumptions. In the case of Figure 11, most noise signals are long, thin edges that are relatively straight. It is a reasonable assumption that a fire plume will not be detected as a long, thin, and straight line. This spatial assumption could disqualify most false positives in the scene based on this criterion without reducing the signal strength of the heat plume, or overall sensitivity. Kohler chose to only apply detection algorithms to MWIR because of the ability to detect smoke signal. It would probably perform better to use LWIR since the smoke signal is not a necessary component for detecting a heat plume.

3.3 Davenport

3.3.1 Summary

Tim Davenport's thesis [6] studies the spectral, temporal, and spatial attributes of a smoke plume. Davenport applies PCA to single instance multi-spectral images and to multi-instance, multi-spectral images. The PCA of 5-band (visible, MWIR, and LWIR) was unsuccessful in exploiting the smoke plume. The more successful spectral-temporal-PCA was able to identify a smoke plume in PC7 after texture analysis. Texture is characterized by statistical descriptors derived from the PC's joint probability density distribution within a spatial relationship. This descriptor is known as a Gray Level Co-Occurrence Matrix (GLCM). Texture analysis is performed on PC7 in order to produce a quantitative sum of GLCM correlation value. Davenport shows that the sum of GLCM correlations above a threshold of 0.5 can effectively classify the presence of a smoke plume in a scene. While smoke plume segmentation has been demonstrated with PCA of IR images, the addition of GLCM texture classification reduced noise

and false positives in the segmentation results. This method was chosen for deeper consideration in Chapter 4 of this paper.

3.3.2 Review

Davenport attempts multispectral PCA using 5 input images (R, G, B, MWIR, and LWIR). The first pass of 5-image, single instance PCA reveals an unevenness. The author identifies the 14-bit range of IR to overweigh the PC output images, so these images are corrected using a Z-score normalization scheme. The original histograms in Figure 17 demonstrate the 14-bit range of IR images. The Z-score normalization histograms are displayed in Figure 18. The author also accounted for nonlinearity of IR images and used gamma mapping to correct the histograms. Figure 19 shows the histograms after gamma mapping and Z-score normalization. The remainder of Davenport's paper will use nonlinear mapping for analysis and smoke plume detection.

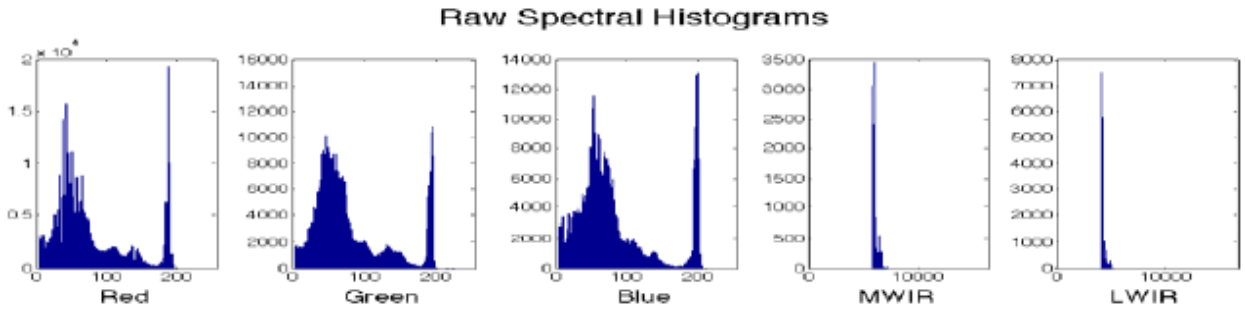

Figure 17 - Histograms before normalization. Source: Davenport Figure 6

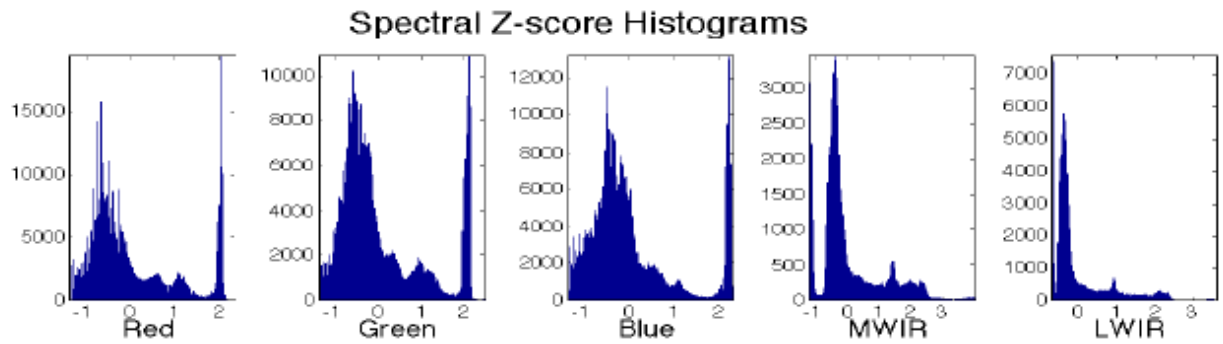

Figure 18 - Z-score corrected histogram. Source: Davenport Figure 11

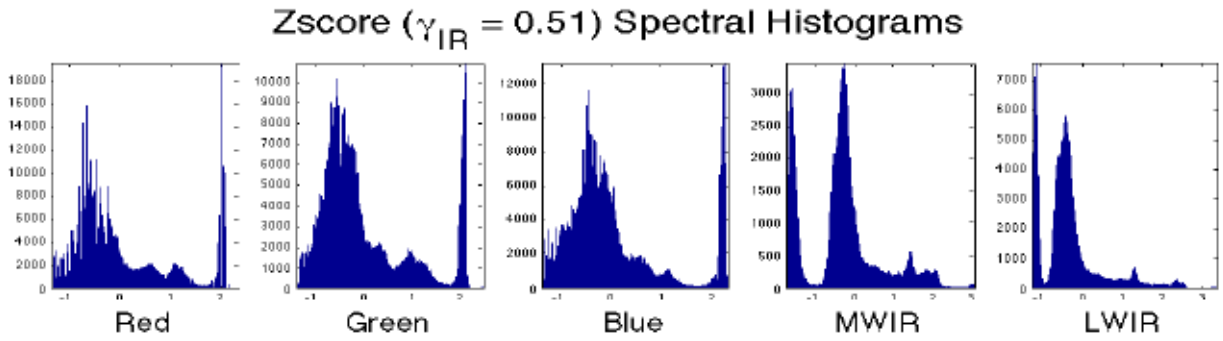

Figure 19 - Gamma Mapping and Z-score normalization. Source: Davenport Figure 19

The author experiments with Temporal-Spectral PCA as a smoke plume detector using 2 time instances and 5 spectral bands to produce a 10 PC images. By adding the temporal dimension, smoke appears in PC7; however, this PC shows moving objects such as two passing vehicles, as observed in Figure 20. The author also shows that PC7 is mostly contributed to by images in the visible spectrum in Figure 21.

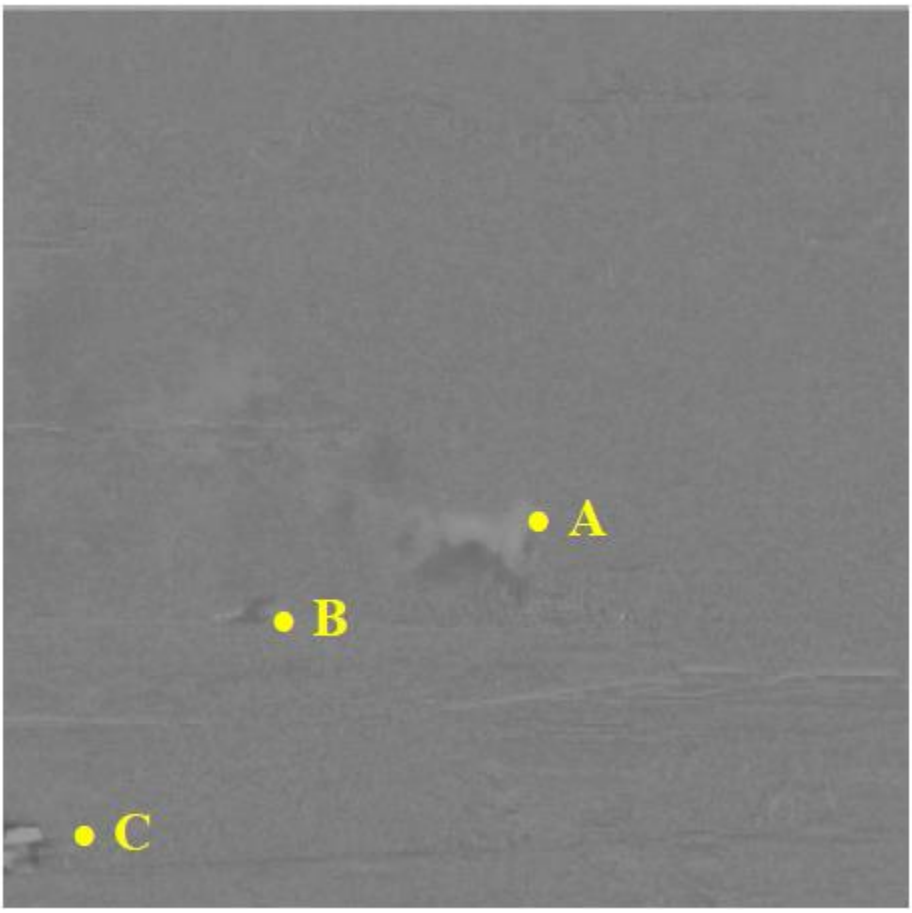

Figure 20 - PC7 of 2 Time Instance Temporal-Spectral PCA. (A) Smoke Plume, (B) Car, (C) Truck. Source: Davenport Figure 27

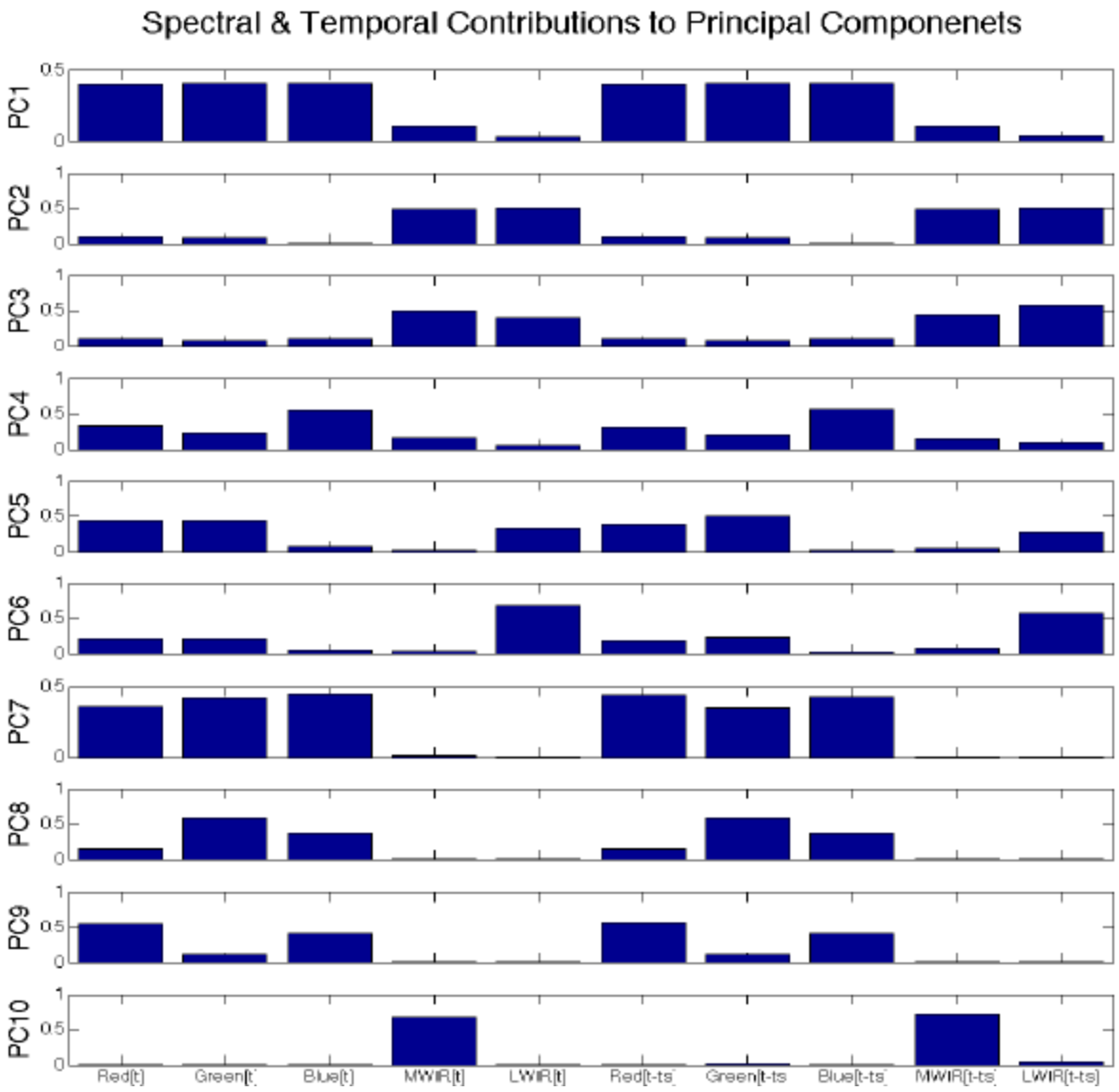

Figure 21 – Magnitude of PCA loadings from each dimension of the Spectral/Temporal image set.

Source: Davenport Figure 28

It is noticed in PC7 that the texture of the smoke plume is uniform compared to the background and other objects. Texture analysis is explored as a way to segment the smoke plume in the PC7 image. Gray Level Co-Occurrence Matrix Texture Analysis is used to identify spatial similarity. The GLCM is calculated in four directions. The resulting GLCM are shown for the given PC7 image in Figure 22.

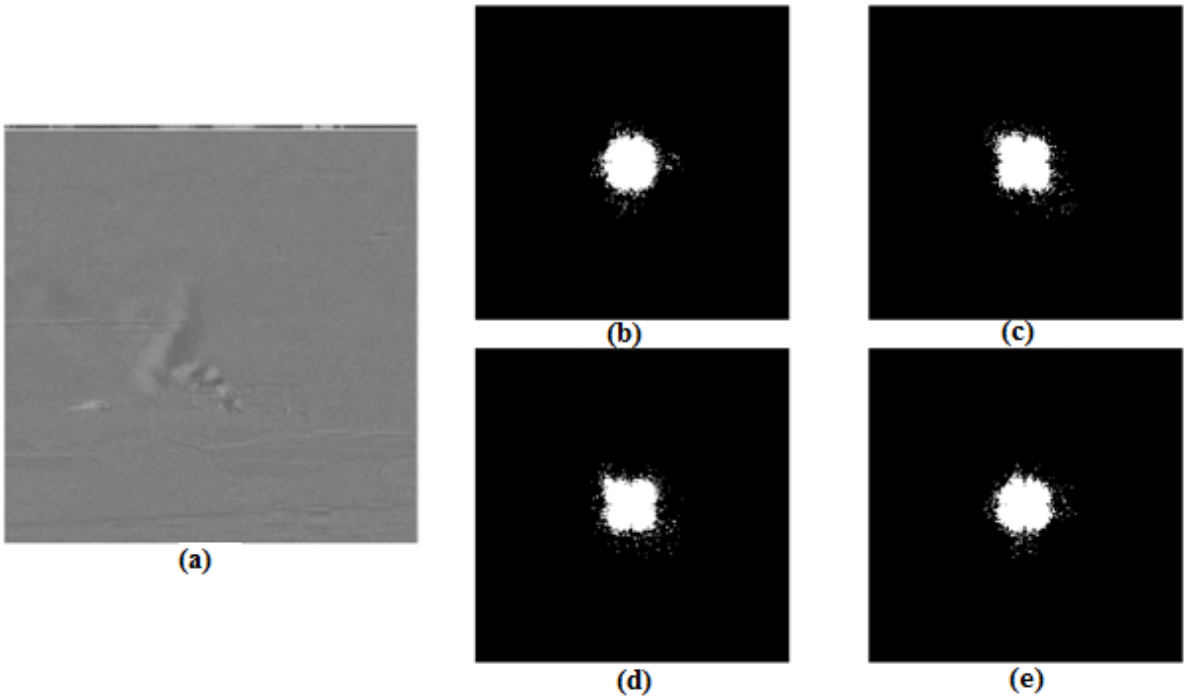

Figure 22 – Gray Level Co-Occurrence Matrixes, (a) PC7, (b) [-20, -20], (c) [-2, 0], (d) [0, -2], (e) [6, 16].

Source: Davenport Figure 34

From each GLCM, four statistical features are analyzed (Contrast, Correlation, Energy, and Homogeneity). For a highly random image, nearby pixels are expected to be uncorrelated, and non-uniform. Conversely, an image with pixels of the same texture will display high correlation, even in spatially distant pixels. GLCM texture descriptors are evaluated over time in 3-instance, 5 band PCA. When the summation of texture descriptors are made over the image, it is apparent that correlation demonstrates a growing trend that matches the smoke growth at the same time in the image sequence, see Figure 23. Figure 24 demonstrates the usefulness of overall correlation as a texture descriptor for smoke plumes.

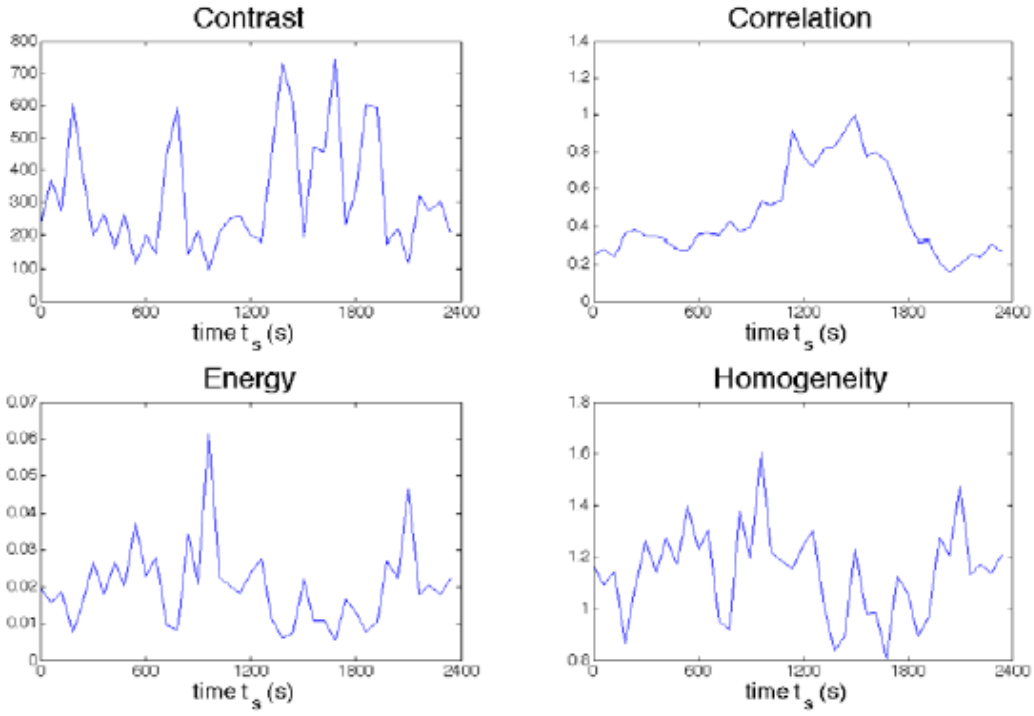

Figure 23 - Texture Descriptors over Time of 7th PC GLCMs. Source: Davenport Figure 37

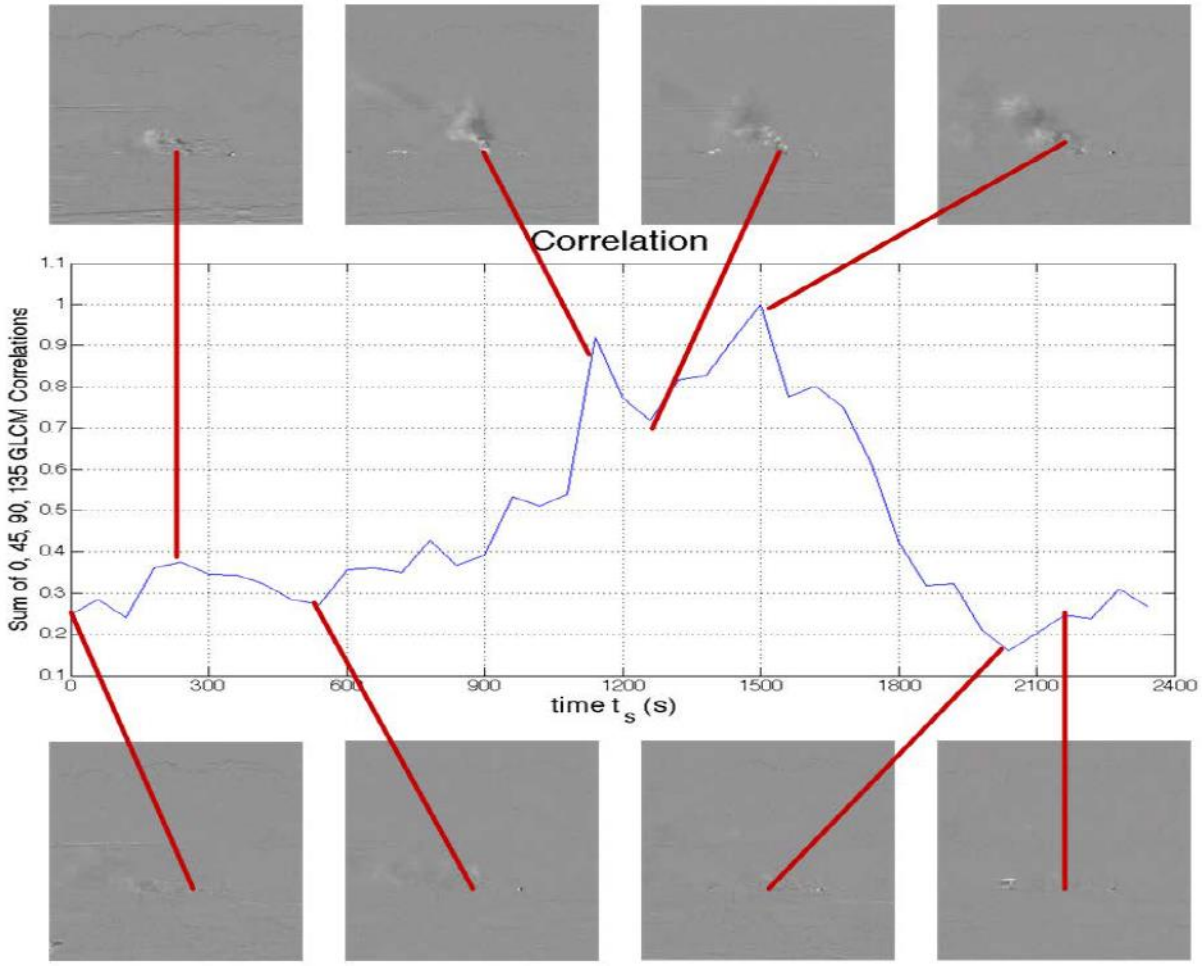

Figure 24 – GLCM Correlation for 7th PC showing start, continuation, and end of smoke plume life. The images correspond to the points in time drawn on the correlation plot. Source: Davenport Figure 40

3.3.3 Suggestions

Since smoke is most prominent in the visible blue spectrum, the method of PCA + GLCM + Correlation could be very successful if restricted to only the visible blue spectrum. The results in Figure 24 visually demonstrate how effective this detection scheme is, and one can only assume that results would improve by removing LWIR, MWIR, visible green, and visible red.

3.4 Aldama

3.4.1 Summary

Raul-Alexander Aldama's thesis [7] aims to exploit the spectral differences between LWIR and MWIR due to CO2 emission and absorption. A number of spectral domain pre-processing methods are explored, namely differencing LWIR and MWIR (called difCLCM). Aldama presents the design of a neural network for detecting a heat plume using LWIR and MWIR video. The author does not adequately demonstrate the success of the chosen design, making assessment challenging. PCA processing of spectral pre-processed frames is explored in an attempt to show that PCA is costly and not as good as multispectral differencing for heat plume detection. A comparison of methods identifies difCLCM as the method with the lowest overall error rate. This method is explored in more detail in Chapter 4 of this paper. The most valuable techniques of this system are the simplicity of spectral differencing, and the effectiveness of input mask filtering. A downside to this design was the necessity to train the neural network with a large data set, and that was one of the reasons for the lack of success.

3.4.2 Review

Aldama attempted to design a simple scheme for heat plume detection that didn't require the complexity of PCA, but relied on the inherent properties of LWIR and MWIR. The cooled, MWIR + LWIR camera has co-located detectors, so they benefit in having the same FOV, bit-depth, resolution and do not require image registration.

Frame processing method experiments determined the best methods for exploiting the heat plume signal. Spectral differencing, referred to as diffCLCM, was chosen as the best method for suppressing noise and highlighting plume signal, see Figure 25.

Figure 25 – “Oats1” difCLCM output. Source: Aldama Figure 52

Noise signals in such as the bright sky and thermal signal of rooftops are the prominent noise in difCLCM frames. These noise signals are believed to be low frequency noise. On the other hand, the heat plume signal shows strong edges that should be immune to a High Pass Filter. Unsharp Mask Filtering is a type of High Pass Filter. First, a Gaussian kernel is convolved with the original image to create a blurred version of the original. Second, the blurred image is subtracted from the original image to create the output image. The Unsharp Filtered image emphasizes the High Frequency components in the difCLCM image. Figure 26 shows the output image from the filter, and Figure 27 shows the efficacy of the filter at attenuating low frequency sky and rooftop signals.

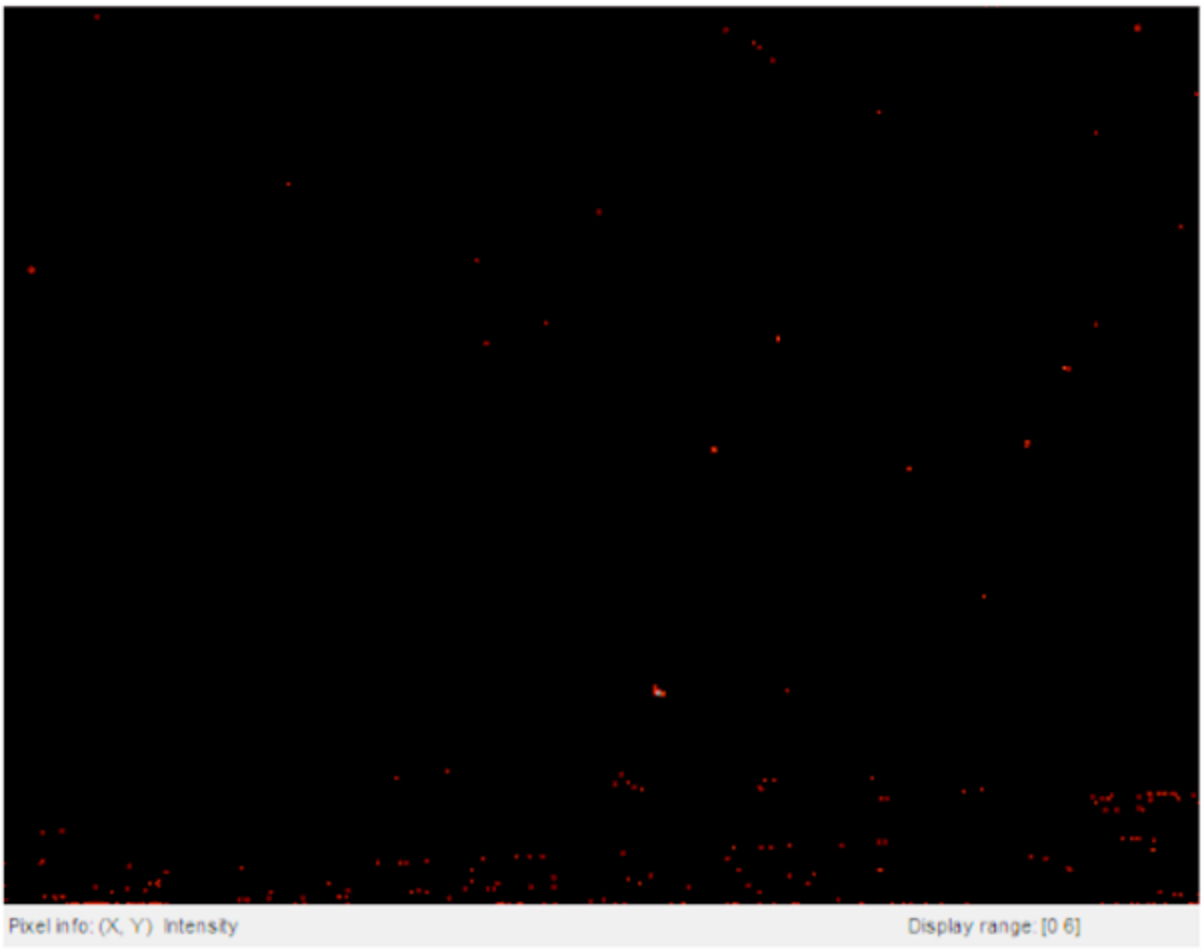

Figure 26 - Unsharp Mask Filter applied to difCLCM “Oats1” frame 1201. Source: Aldama Figure 76

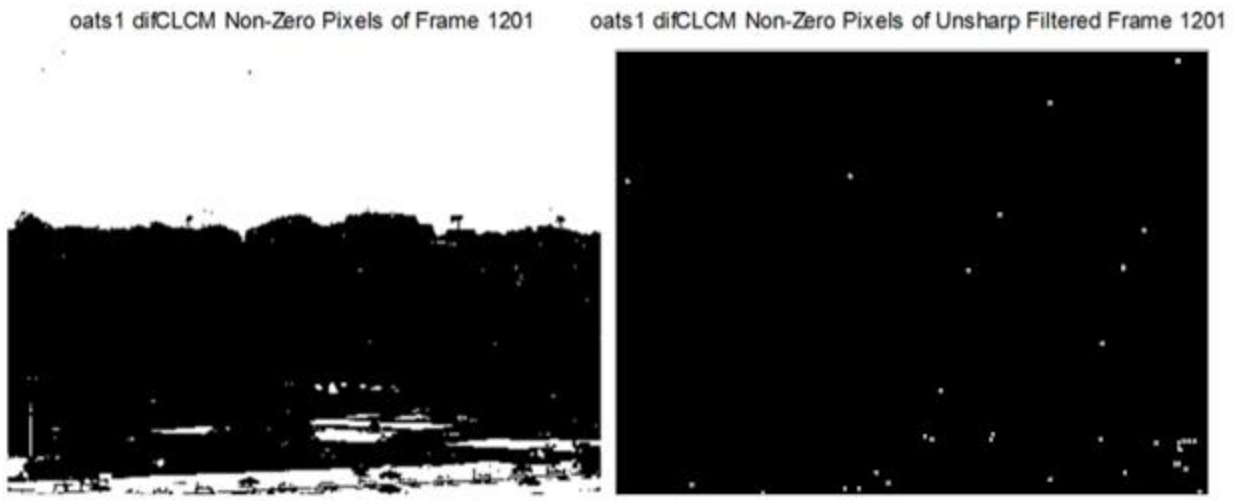

Figure 27 – "Oats1" difCLCM Non-Zero Pixels before and after Unsharp Mask Filtering. Source: Aldama Figure 78

Since there are still false positives, further filtering is needed. The author made the observation that a heat plume shouldn't exist in pixels known to be sky, or otherwise known for low IR intensity. This is the premise for the Input Masking filter that rejects detection points outside the input mask that consists of the 97% intensity threshold image from MWIR. Results of Input Mask filtering are shown in Figure 28, where rejected noise pixels are circled in red (above the horizon), non-rejected points are circled in blue, the fire core is double-circled in blue, and the input mask is shown in purple.

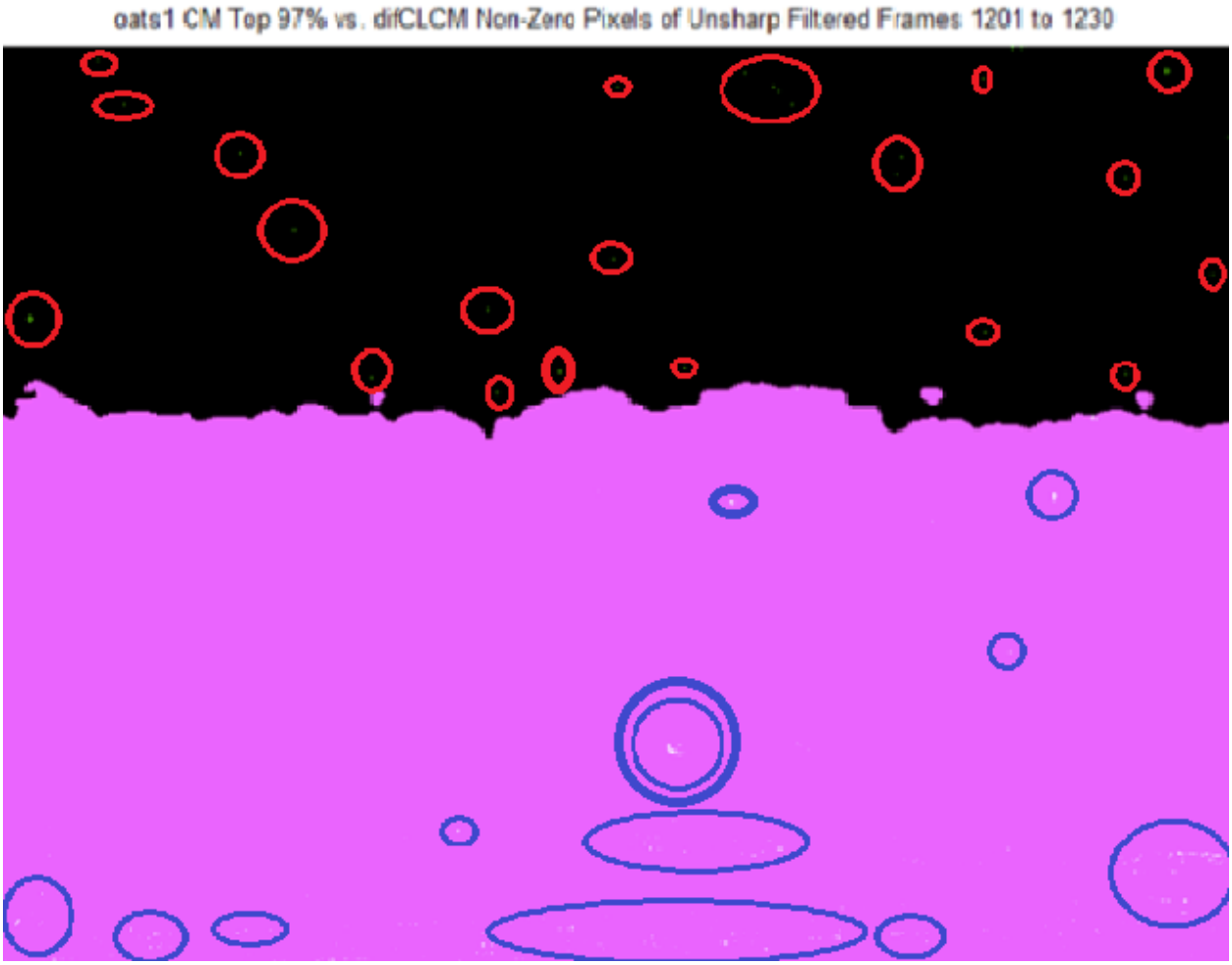

Figure 28 - Input Mask Filtering applied to “Oats1”. Source: Aldama Figure 81

A multilayer perceptron neural network is designed using feature points generated from the ‘oats1’ difCLCM, threshCL, adapthreshCL, and CL processed frames for training. Feature points were calculated by analyzing Neighborhood Standard Deviation, Neighborhood Mean, and Neighborhood Average Auto Correlation. Supervised batch learning was used to train the NN, with the Levenberg-Marquadt algorithm chosen for fast convergence speed and MATLAB efficiency. MWIR frames were not included as training data because they proved unhelpful in classification.

Results were evaluated by three criteria: time to earliest successful detection (see Figure 29), detection error (see Figure 30), and computation time (see Figure 31). ‘difCLCM’ outperformed all other frame processing methods in all metrics, except time to earliest successful detection, where other methods performed as well. The success of difCLCM can be attributed to the high IR intensity that is visible in all fuel-type scenes, except ‘charcoal1’. However, the poor results of ‘charcoal1’ can be expected since it was the first fuel source and the temperature is expected to be lower of the fire and the radiating sources around the fire.

Process	Gaussian Kernel Sigma	Successful Detection Time (seconds)
difCLCM	**0.25**	**1**
threshCL	0.218	19
adapthreshCL	0.218	6
CL	**0.24**	**1**
CM	0.24	-
pcadifCLCM	**0.216**	**1**
pcathreshCL	0.218	25
pcaadapthreshCL	0.218	20
pcaCL	**0.24**	**1**
pcaCM	0.24	-
pcaCLCM	**0.24**	**1**
pcaTCLCM	**0.25**	**1**

Figure 29 - Time to Earliest Successful Detection. Source: Aldama Table 8

Process	Detection Failure	Detection Failure Error	False-Negatives	False-Negative Error	False-Positives	False-Positive Error	Error Sum
difCLCM	**0**	**0.0000**	**0**	**0.0000**	**0**	**0.0000**	**0.0000**
threshCL	37	0.5286	15	0.2143	0	0.0000	0.7429
adapthreshCL	25	0.3571	20	0.2857	0	0.0000	0.6428
CL	0	0.0000	2	0.0286	5	0.0714	0.1000
CM	64	0.9143	6	0.0857	0	0.0000	1.0000
pcadifCLCM	1	0.0143	3	0.0429	1	0.0143	0.0715
pcathreshCL	39	0.5571	20	0.2857	0	0.0000	0.8428
pcaadapthreshCL	4	0.0571	43	0.6142	1	0.0143	0.6856
pcaCL	9	0.1286	1	0.0143	1	0.0143	0.1572
pcaCM	63	0.9000	7	0.1000	0	0.0000	1.0000
pcaCLCM	2	0.0286	2	0.0286	0	0.0000	0.0572
pcaTCLCM	5	0.0714	3	0.0429	1	0.0143	0.1286

Figure 30 - Detection Error. Source: Aldama Table 9

Process	Computation Time (seconds)
difCLCM	**0.208992**
threshCL	0.342265
adapthreshCL	1.768455
CL	-
CM	-
pcadifCLCM	7.493135
pcathreshCL	7.553252
pcaadapthreshCL	7.771184
pcaCL	7.488735
pcaCM	7.48570
pcaCLCM	5.286425
pcaTCLCM	12.438535

Figure 31 - Computation Time. Source: Aldama Table 12

3.4.3 Suggestions

Overall, the novel utility of Aldama's proposed heat plume detection system is filtering thermal signals such as rooftops and sun reflections, while remaining unaffected by macro-

movements such as cars. The application of Unsharp Mask filtering and Input Mask filtering can be applied in many other detection schemes as pre-processing steps. While the author experimented with adjusting video registration and Gaussian kernel sigma parameters to achieve improved outcome from the NN, it would be most fruitful to demonstrate the performance of the NN using a much larger training data set. The author made the observation that the training data was weighted towards difCLCM using 'oats1', and this would influence its performance. Does difCLCM input to the NN perform well in detecting other fuel types? Can this technique also be applied to a different scene without acquiring new training data in that scene?

3.5 Boynton

3.5.1 Summary

Ansel Boynton's thesis [8] designs a heat plume detection algorithm from MWIR and LWIR video. Temporal filtering is applied to infrared video to remove a background image and periodic signals created by camera movement. A bandpass filter and a high pass filter reduce noise and motion artifacts caused by tower sway. A Gaussian blur also reduces motion artifacts. After applying the digital filters and Gaussian blur to LWIR and MWIR frames, classification is performed on a segmented image. The use of assumptions for classification is strong in Boynton's design. While simple, it is very powerful to use the assumption of size, eccentricity, and relative power of LWIR over MWIR to classify a heat plume. Filtering out motion artifacts caused by motion sway requires applying a bandpass filter that unfortunately also removes significant energy in the IR spectrum.

3.5.2 Review

Boynton designs a heat plume detection system using frequency domain filtering and spatial filtering. The initial step was to analyze the frequency profile of various signals in a fire scene in LWIR and MWIR. The following signals were inspected in the frequency domain: saturated fire, building fire, strong edge, uniform surface, textured surface, and moving object. Analysis of a saturated fire contains no frequency data since the detector saturated and the clipping distorts the DFT. Analysis of the building fire reveals less power at distant points from the fire core, these results are shown in Figure 33. Frequency analysis of a uniform surface demonstrates spikes at 0.95 Hz and 2.9 Hz, which is later explained as the resonant frequency induced by the swaying tower upon which the cameras were mounted. The author then aims to design a bandpass filter between the resonant motion frequencies for the fire detection system.

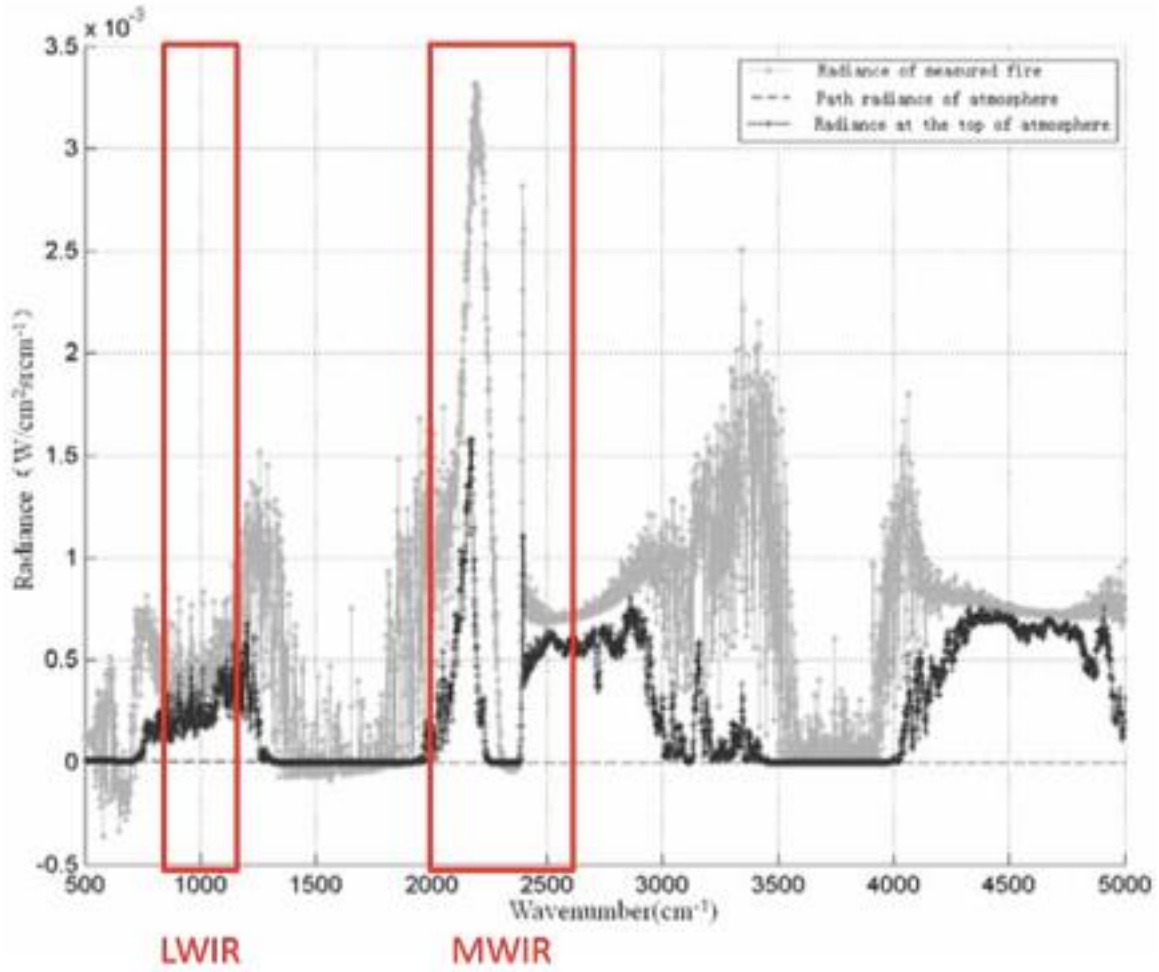

Figure 32 - Radiance of Forest Fire in the IR Spectrum. Source: Boynton Figure 5

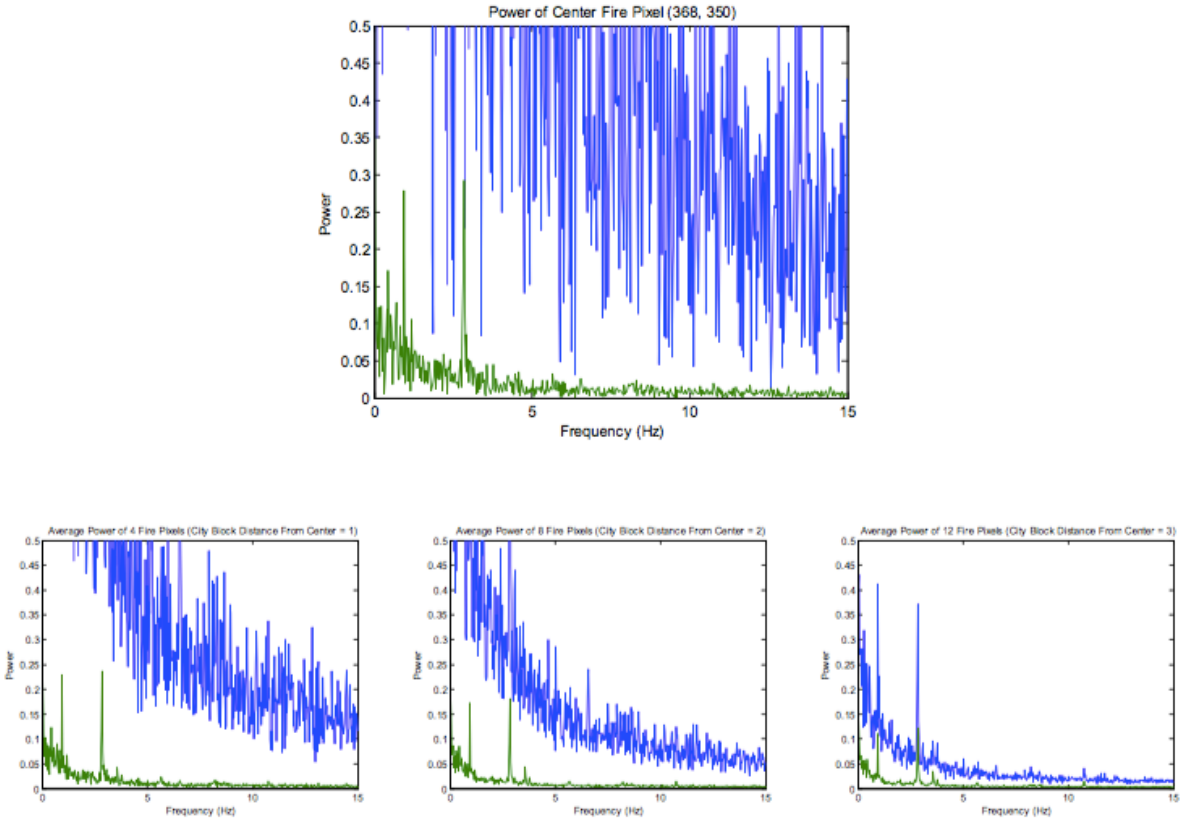

Figure 33 - Frequency Profile of Points in a Fire Scene (MWIR in Green, LWIR in Blue). Source: Boynton Figure 10

As stated above, a bandpass filter between 0.95 Hz and 2.9 Hz will filter out motion sway. In addition, a High Pass Filter will be applied to reduce noise. A Gaussian Blur will also be applied to reduce high frequency content of edges caused by swaying. A FIR High Pass Filter was designed and the coefficients are shown in Figure 34. The design of the IIR Band Pass Filter is discussed next, and a major design consideration is the cost-benefit of filter length vs group delay, as demonstrated in Figure 35.

$$y[0] = \sum_{0}^{28} B_k * x[-k] \ where:$$

$$B_k =$$

k	B_k value	k	B_k value	k	B_k value
1	-0.00083	12	-0.09205	22	-0.00556
2	0.002179	13	0.113571	24	0.008271
3	-0.00423	14	-0.12817	25	-0.00855
4	0.006682	15	0.133333	26	0.006682
5	-0.00855	16	-0.12817	27	-0.00423
6	0.008271	17	0.113571	28	0.002179
7	-0.00407	18	-0.09205	29	-0.00083
8	-0.00556	19	0.067096		
9	0.021271	20	-0.04245		
10	-0.04245	21	0.021271		
11	0.067096	23	-0.00407		

Figure 34 - FIR High Pass Filter Equation and Coefficients. Source: Boynton Equation 7

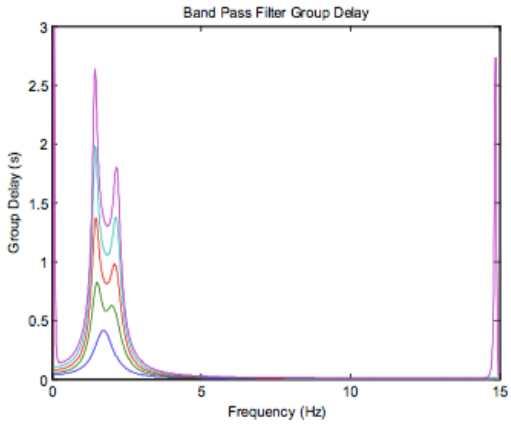

Order	Color	Max Pass Band Group Delay (sec)	Ave. Pass Band Group Delay (sec)
1	Blue	0.4165	0.2535
2	Green	0.8202	0.5459
3	Red	1.3687	0.8407
4	Cyan	1.9795	1.1334
5	Purple	2.6348	1.4241

Figure 35 - IIR Band Pass Filter Design. Source: Boynton Figure 27, Table 7

The next step in the filter design is to spatially blur the non-smooth images with a Gaussian Filter. The results at this stage of the system are capable of producing a binary image that is segmented and objects are sorted into groups using connected component analysis, see Figure 36.

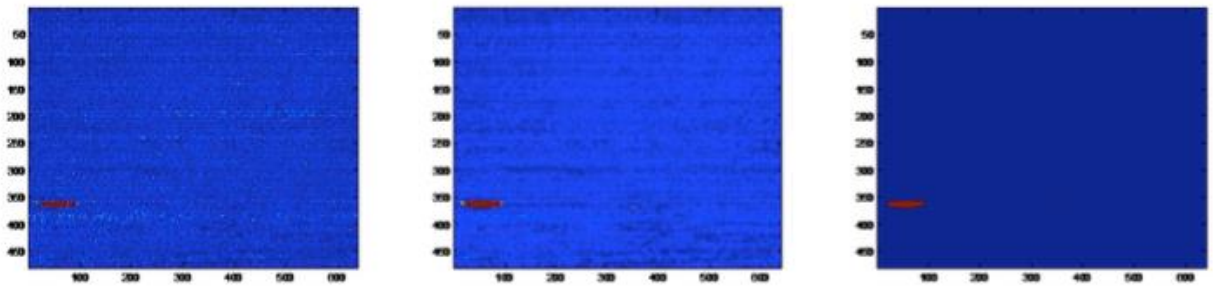

Figure 36 - Gaussian Blur producing Binary Image. High Pass Original Image (Left), Blurred Image (Center), and Binary Image (Right). Source: Boynton Figure 32

The segmented regions are then classified as fire or non-fire by intuitive feature analysis. The regions must resemble a fire by the following attributes: size, eccentricity, and LWIR power vs. MWIR power. The decision tree is shown in Figure 37, and the justification for relative power comparison in LWIR and MWIR is shown in Figure 38 and Figure 39.

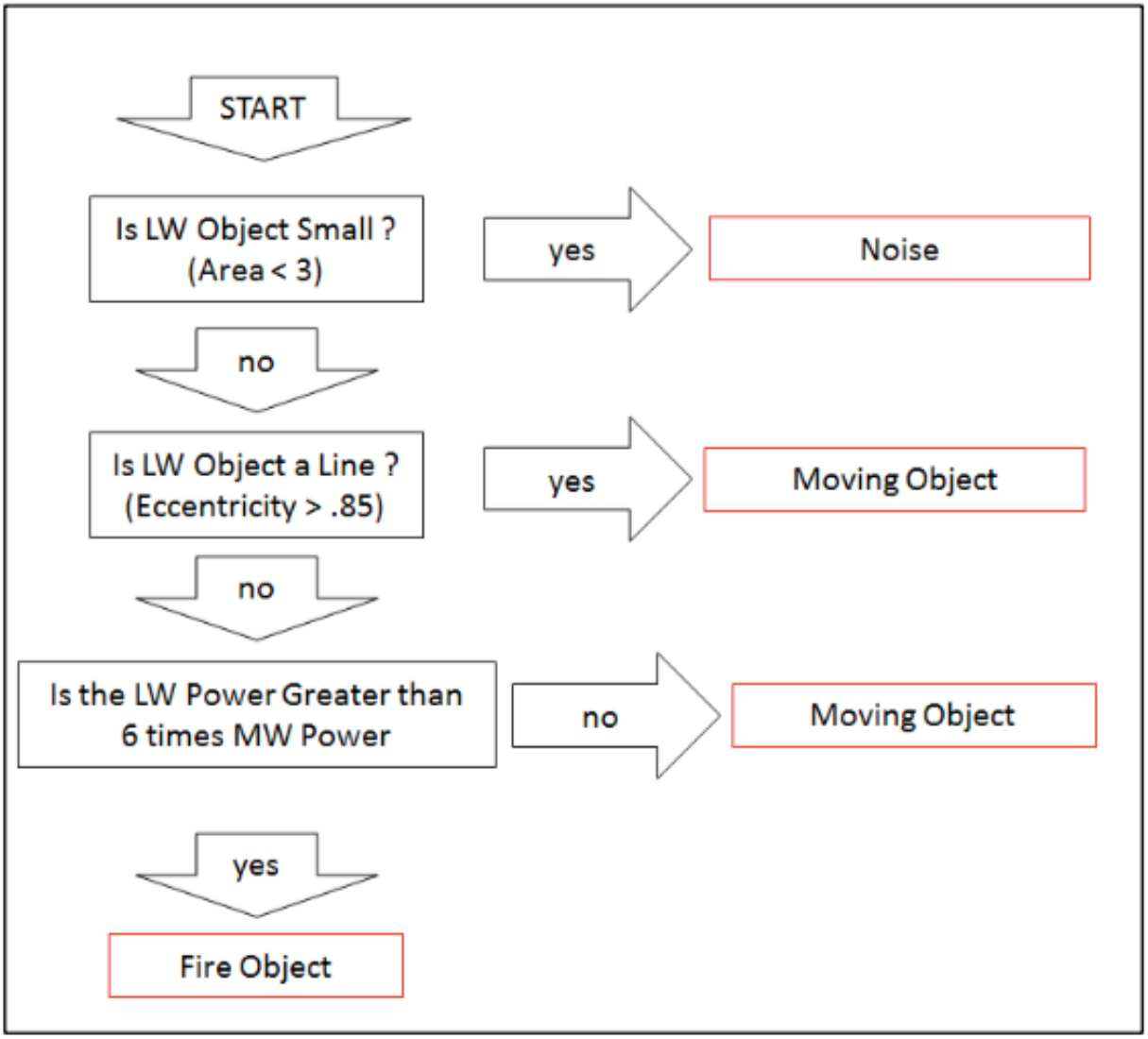

Figure 37 – Decision Tree for Detected Objects. Source: Boynton Figure 33

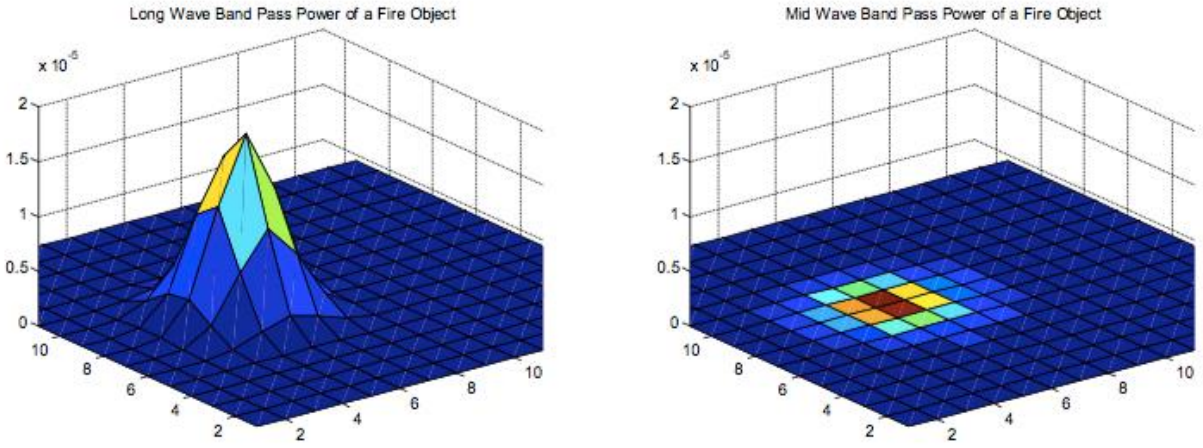

Figure 38 - LWIR vs. MWIR Power of a Small Fire. Source: Boynton Figure 35

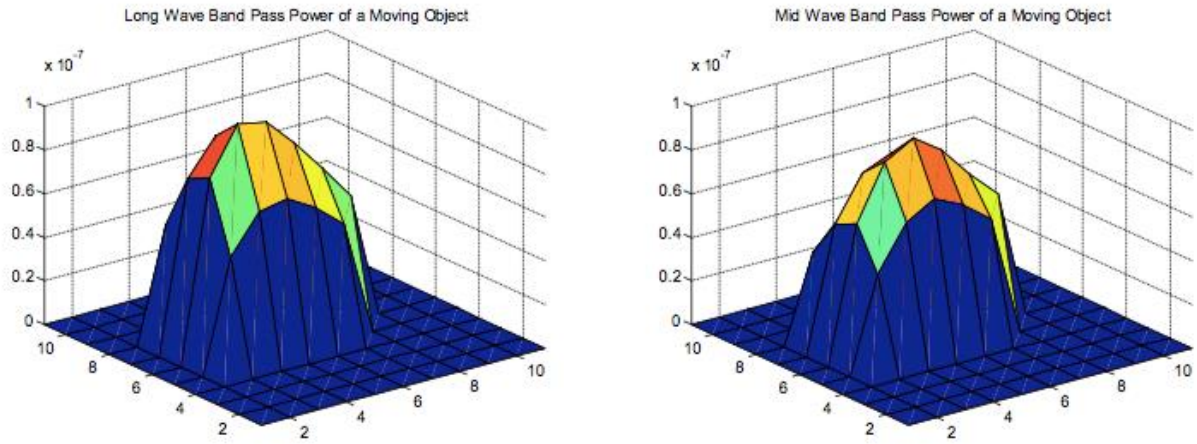

Figure 39 - LWIR vs. MWIR Power of a Moving Object. Source: Boynton Figure 36

3.5.3 Suggestions

One way to improve the detection scheme is to modify the Gaussian Blur filter applied. The design choice was made to use equal standard deviations for the horizontal and vertical directions, but it makes sense to blur the horizontal direction more, since this is the movement direction of the majority of tower sway. A drawback in bandpass filtering to remove motion

artifacts is that it removes significant energy in the IR spectrum. While Boynton is designing around the limitations of the acquired data, it would be an improvement to place a camera on a stable structure that won't impart as much sway. This should increase the sensitivity of Boynton's system.

3.6 Garges

3.6.1 Summary

David Garges's thesis [9] presents two methods for segmenting smoke from visible blue images. The cumulative differencing method was concluded to be unsuccessful due to its high false positive rate. The successful method was PCA followed by blurring, adaptive thresholding, and median filtering. While, this method was said to perform better than the cumulative differencing method, the author provided little evidence of this comparison. One drawback to this method is that the adaptive threshold technique requires a manual tuning constant that is derived from the fire scene. This parameter is sensitive to the fire location's distance from the camera, as well as wind in the scene. Another drawback is that the technique relies on temporal variance of visible images; thus, many noise signals (motion of birds, trees, or vibrations) create false positives. Thankfully, the size of smoke typically dominates these noise sources.

3.6.2 Review

Garges presents a successful application of PCA on visible blue images, followed by spatial filtering to segment a smoke plume. Garges's research used data from the 2012 Goleta Fire Experiment. Garges finds that the best results come from PCA of 5 visible blue images, separated by 2 seconds, and with a tuning constant of 4.5. The tuning constant determines the

acceptable level of temporal variance. The threshold process is applied to a blurred principal component image.

The author tests the ability to separate smoke from non-smoke using feature space analysis. RGB and HSV color space analysis are unable to definitively identify smoke without creating false positives. The lack of separability is shown in RGB, HS, and SV analysis, shown in Figure 40, Figure 41, and Figure 42, respectively.

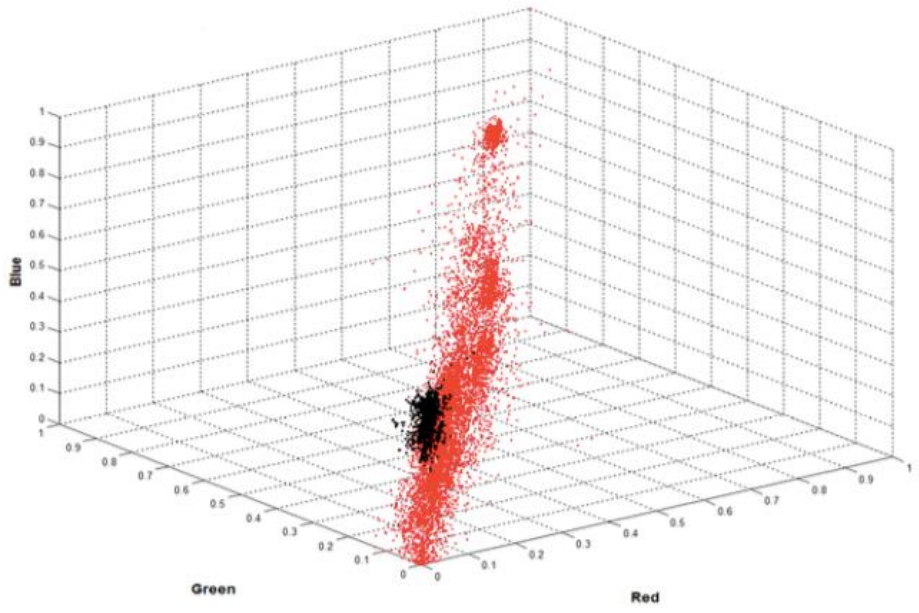

Figure 40 - RGB Color Space Analysis showing Feature Space of Fire Scene. Source: Garges Figure 16

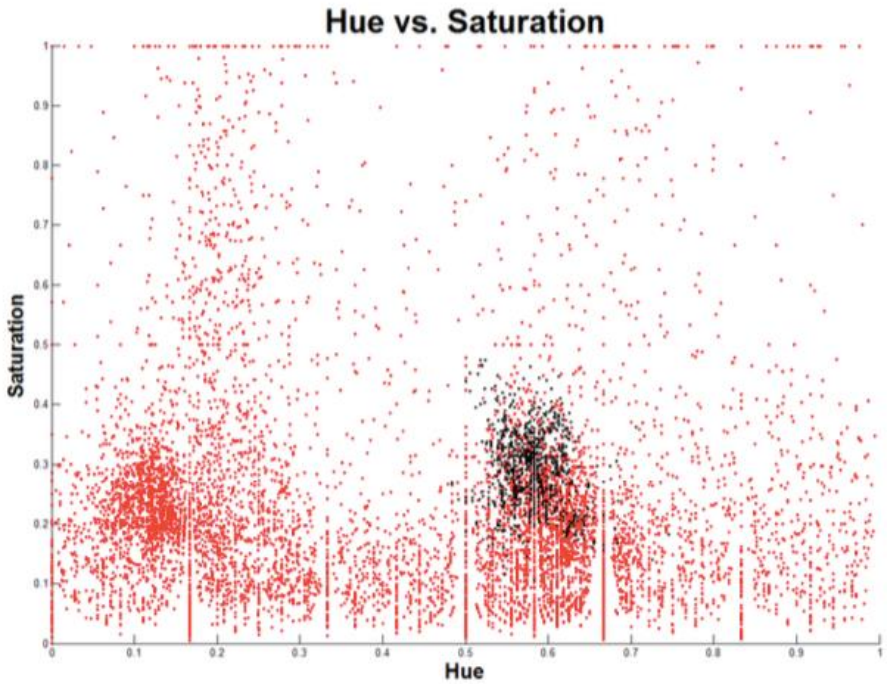

Figure 41 – Hue vs. Saturation of Fire Scene. Source: Garges Figure 19

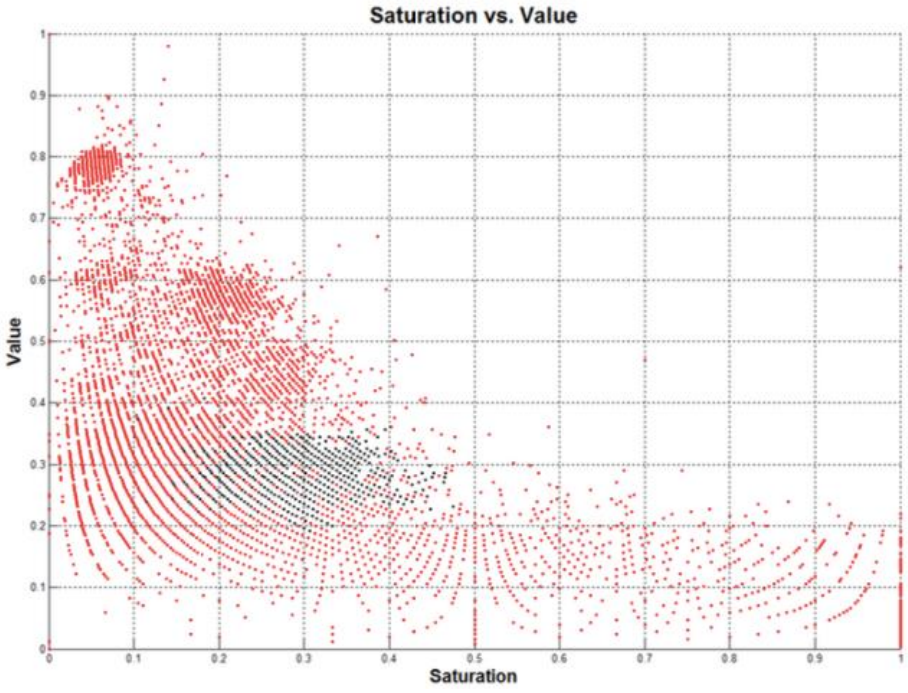

Figure 42 – Saturation vs. Value of Fire Scene. Source: Garges Figure 20

In Chapter 5 of the paper, the author attempts to identify smoke by image differencing. Differencing is a pixel-wise subtraction of two images. This method is an easy way to segment a moving object. The visible blue spectrum is chosen for analysis in the remainder of this paper due to its relative separation compared to red and blue images, see Figure 43. A differencing scheme is designed using 5 images at 5 second intervals that involves blurring, manual threshold adjustment, and median filtering. The method for calculating a cumulative difference image is shown in Figure 44. The result of this scheme is shown in the right-most image in Figure 45, where time difference of 5 seconds and 5 total images are input to calculate the cumulative difference image. This method is successful in segmenting large temporal variance, but false positives from movement and edges (likely caused by tower sway) make this method overall unsuccessful and will not be considered further in this paper.

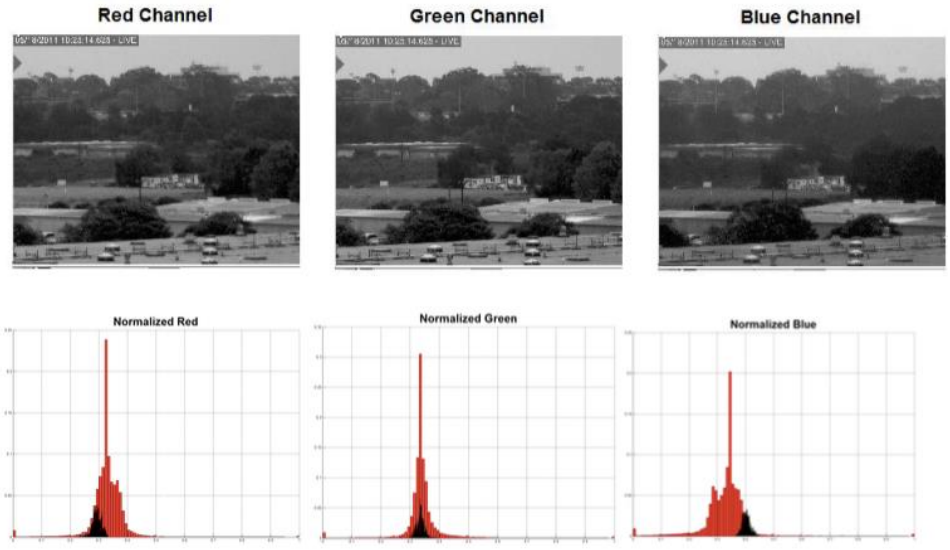

Figure 43 - Separability of smoke in blue channel. Visible Bands Shown above, Histograms Shown below.

Source: Garges Figure 21

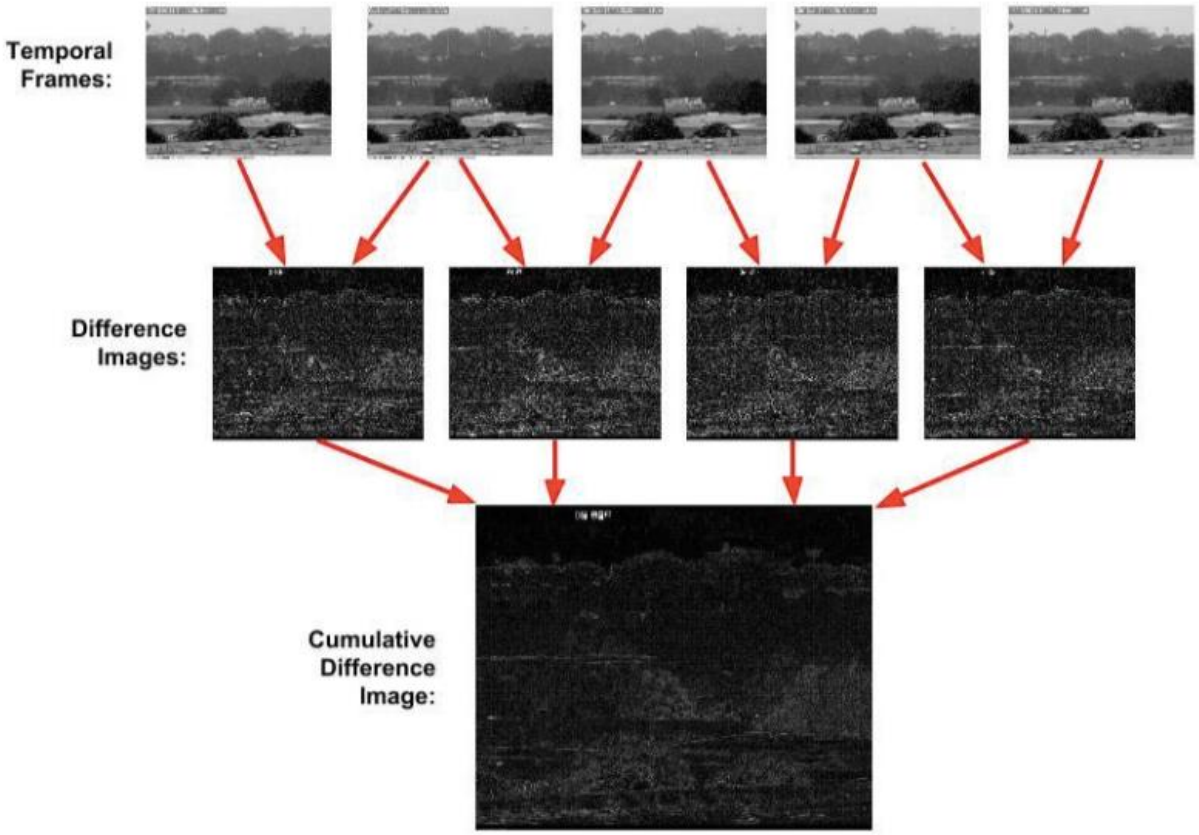

Figure 44 – Construction of Cumulative Difference Image from Temporal Image Sequence.

Source: Garges Figure 22

Figure 45 - Results of Difference Image Method with Delta = 5sec. Source: Garges Figure 26

Chapter 6 of Garges studies the temporal signature of smoke and exploits this with temporal PCA. PCA of temporal images shows that large temporal variance have intensities

outside image mean. Auto threshold adjustment is applied to a PC image. The equation for calculating the manual threshold value is shown in Figure 46, where standard deviation (σ), and intensity mean (μ) are outputs from the Gaussian Mapping stage. The block diagram for the temporal PCA segmentation scheme is shown in Figure 47. The results of this method shows the final segmented image in Figure 48.

$$Theshold = \mu + A * \sigma$$

Figure 46 - Automated Threshold Equation. Source: Garges

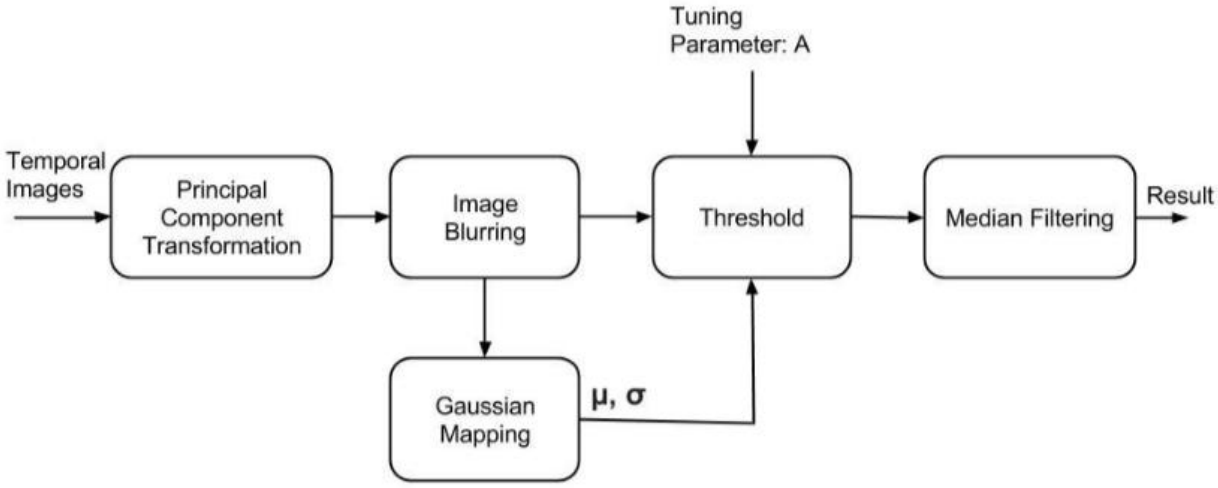

Figure 47 - Block Diagram for Selective Threshold Adjustment on PC Images. Source: Garges Figure 28

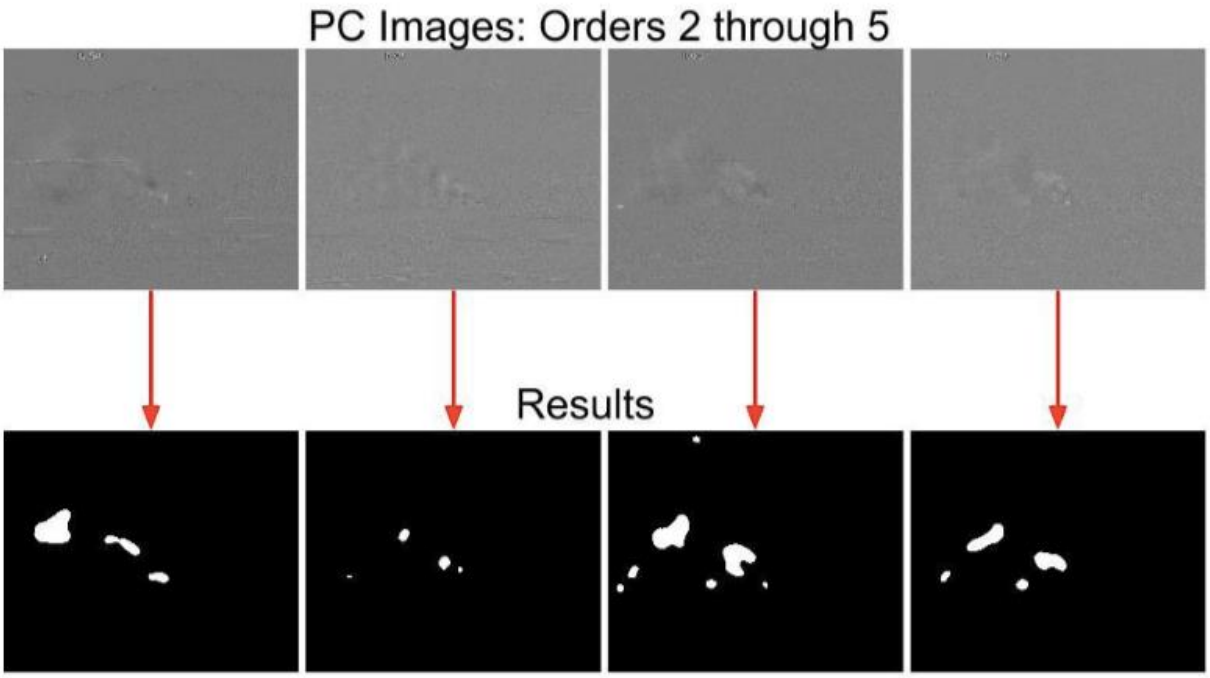

Figure 48 - Segmentation results from Selective Threshold Adjustment of PC Images.

Source: Garges Figure 32

3.6.3 Suggestions

The study concludes that the optimal parameters are a time interval of 2 seconds between images, the spectrum is visible blue, 5 input images are used, and PC image 2 is used for analysis. The resulting PCT computes the signature principal component weightings in Figure 49. The author simplifies the equation based on the low contribution in images 2 and 4. This observation also indicates that the same technique could be applied by using 3 input images with 4 second intervals and using the simplified equation below. Another improvement to this system would be in the tuning of the intensity threshold value by using more true negative images in the training process.

$$I_{Temporal\ Signature} = -.49 * I_1 + -.05 * I_2 + -.27 * I_3 - .01 * I_4 + .82 * I_5$$

Which can be further simplified to:

$$I_{Temporal\ Signature} = -.49 * I_1 + -.27 * I_3 + .82 * I_5$$

Figure 49 - Principal Component Eigenvalues. Source: Garges

4 EXPANDING

This chapter of the paper discusses ways to expand or improve upon the research detailed in Chapter 3. An improvement can be made by combining individual methods to add robustness. Also, a high-level system architecture will be proposed as a real-world implementation of wildfire detection. This system will explain the relationship between cameras, the processing system, and a connection to the internet for human review of detections.

4.1 Comparing Methods

The top 12 methods by all six thesis papers are charted in Figure 50. Six methods are for smoke plume detection and six are for heat plume detection. The two most effective methods from each thesis are grouped by primary method, spectrum, and feature detected. From this chart, it is clear that the best method for smoke detection is PCA of the visible spectrum (particularly blue) and that heat plume detection is best done by analysis of the infrared spectrum.

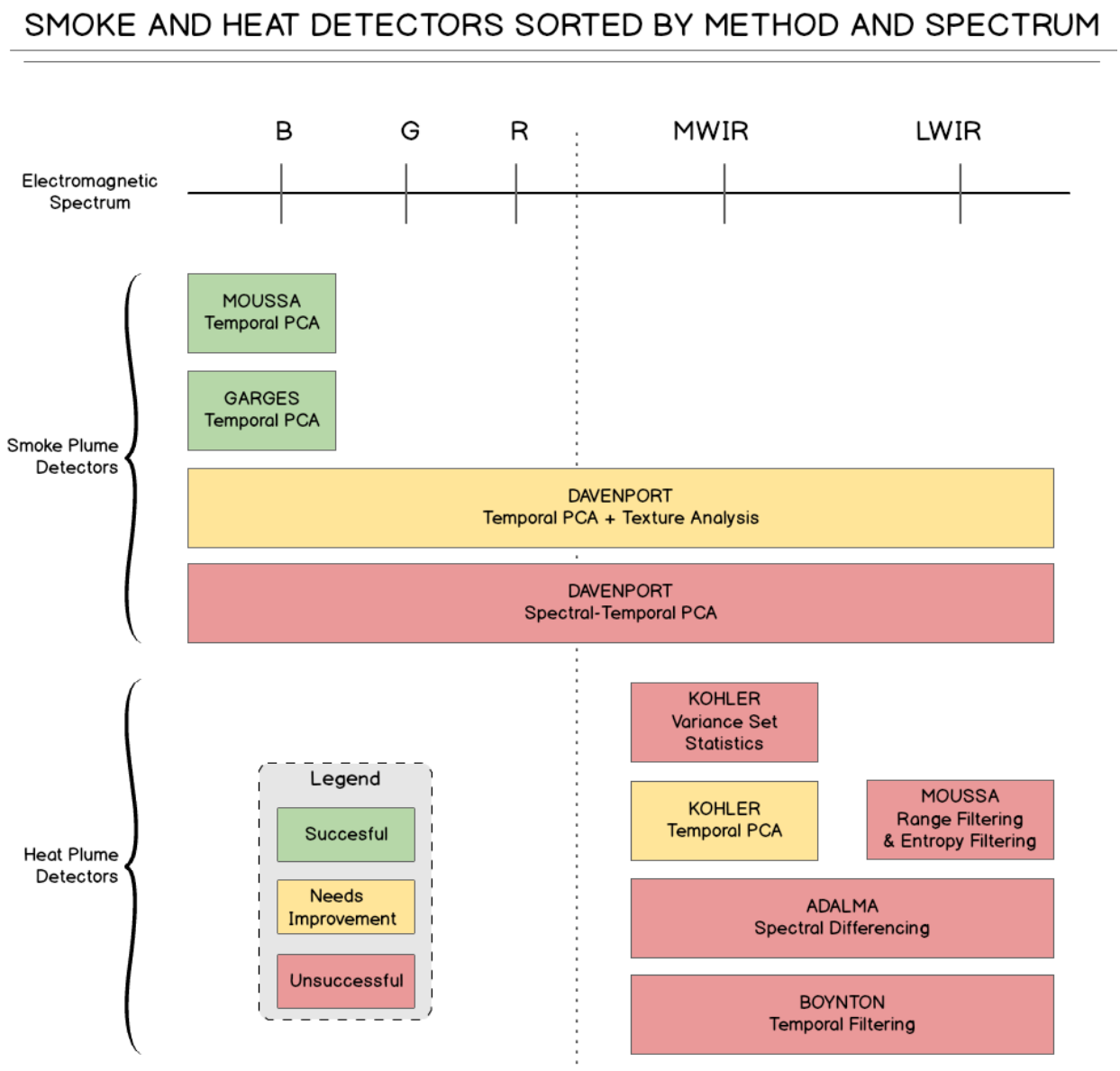

Figure 50 - Summary of Methods Sorted by Spectrum, Author, and Detected Feature

In order to identify the top performers, it is fair to separate Smoke and Heat methods, since no method is fit to identify both signals. Smoke plume detection was attempted with 3 multispectral techniques and 3 by visible blue analysis. A subjective and qualitative ranking of the methods places Moussa's and Garges's PCA of visible blue and Davenport's temporal-spectral- PCA as the three best smoke plume detection techniques.

Heat plume detection was explored only in the infrared spectrum. The qualitatively ranked top-performers were Kohler's PCA of MWIR, Aldama's Infrared Spectral Differencing, and Boynton's Temporal Filtering of LWIR.

4.1.1 Comparing Smoke Plume Detectors

Moussa's PCA of Visible Blue begins with a pre-processing stage that creates the Absolute Blurred PCA input images. This technique is described in Moussa Sec 7.3 [4], "Modification of PC Image to Enhance Smoke Plume Detection". PC2 is post-processed using the Adaptive Thresholding method described in Moussa Sec 6.3, "Threshold and Median Filtering". The results of Adaptive Thresholding of Absolute Blurred PC2 (Figure 51) are demonstrated in Figure 52. The final results of the 10x10 median filtered mask superimposed on the Absolute Blurred PC2 image and the RGB captured image are shown in Figure 53.

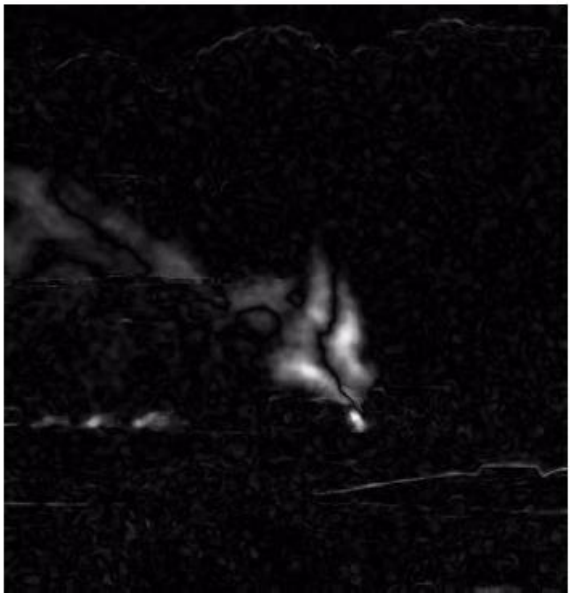

Figure 51 - Absolute Blue Band PC2 of "Oats1". Source: Moussa Figure 61

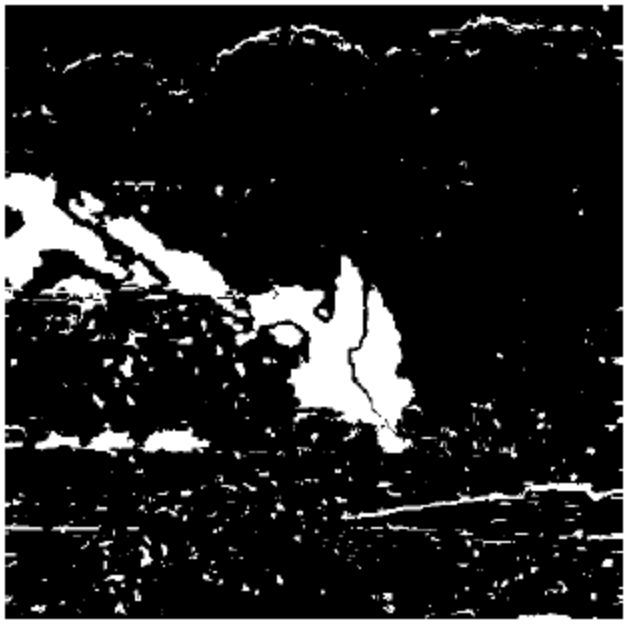

Figure 52 - Adaptive Threshold of PC2 of “Oats1”. Source: Moussa Figure 65

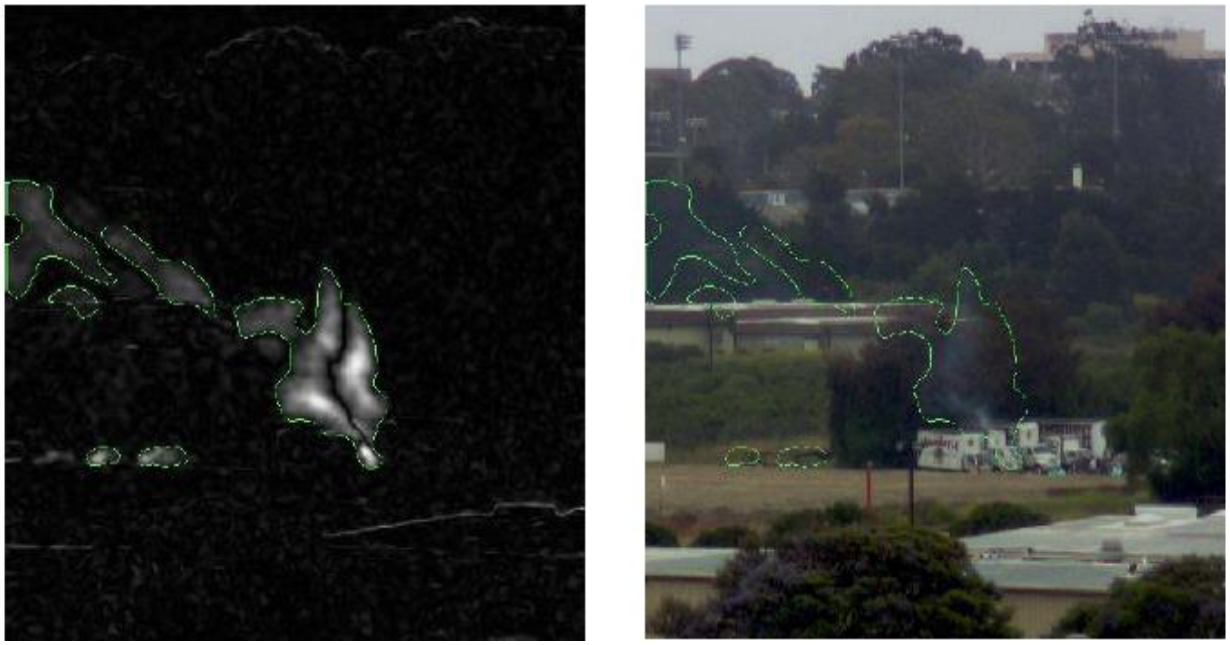

Figure 53 - Segmentation mask superimposed over PC image and RGB image. Source: Moussa Figures 69, 70

An excellent demonstration of this algorithm's detection success over time is to plot segmented blob area moving average over time. The moving average smooths the curve and reduces glitches. Figure 54 displays the results throughout an 800+ frame sequence.

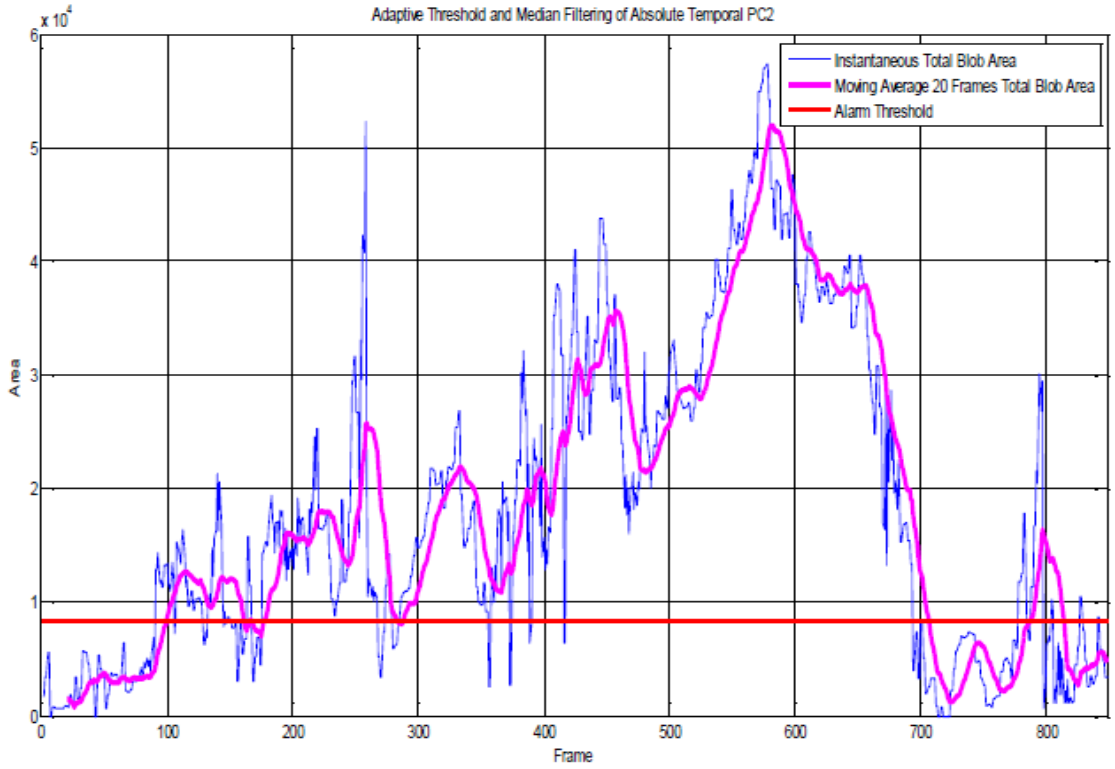

Figure 54 - Smoke plume area growth over time. Source: Moussa Figure 71

In many regards, the merits of Garges's technique are demonstrated in Moussa's technique, however; Garges's deeper study into selecting the optimal parameters for PCA input images is important. Garges concluded on spectrum (visible blue), number of input images (five images), and the interval between images (two seconds). The superiority of visible blue over green and red spectra is demonstrated in Figure 55.

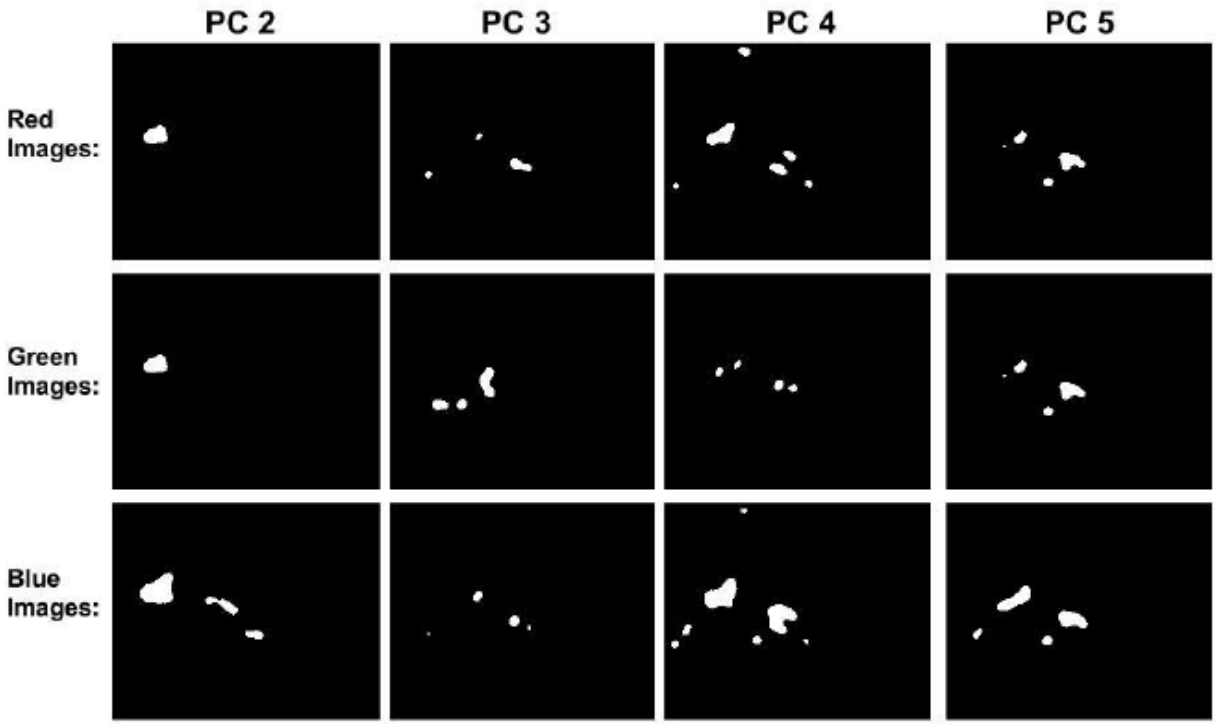

Figure 55 – Comparison of Selective Threshold Adjustment on Visible Channels (used for selection of PC image and color band). Source: Garges Figure 34

Davenport's Temporal-Spectral-PCA is an effective method using the visible spectrum. PC7 alone does not have clearly obvious spatial features required to segment the smoke plume. The next stage of the algorithm is Gray Level Co-occurrence Matrix (GLCM) that is used as a texture descriptor. The uniformity of pixel intensity in the smoke plume region of PC7 is notable, and it properly classifies the presence of a smoke plume. Figure 56 is the best demonstration of how a growing smoke plume translates to a larger correlation value in the image sequence. The time sequence moves left-to-right and top-to-bottom. Thresholding the correlation score effectively classifies the presence of a smoke plume in this method, indicated by a red border around the visible image.

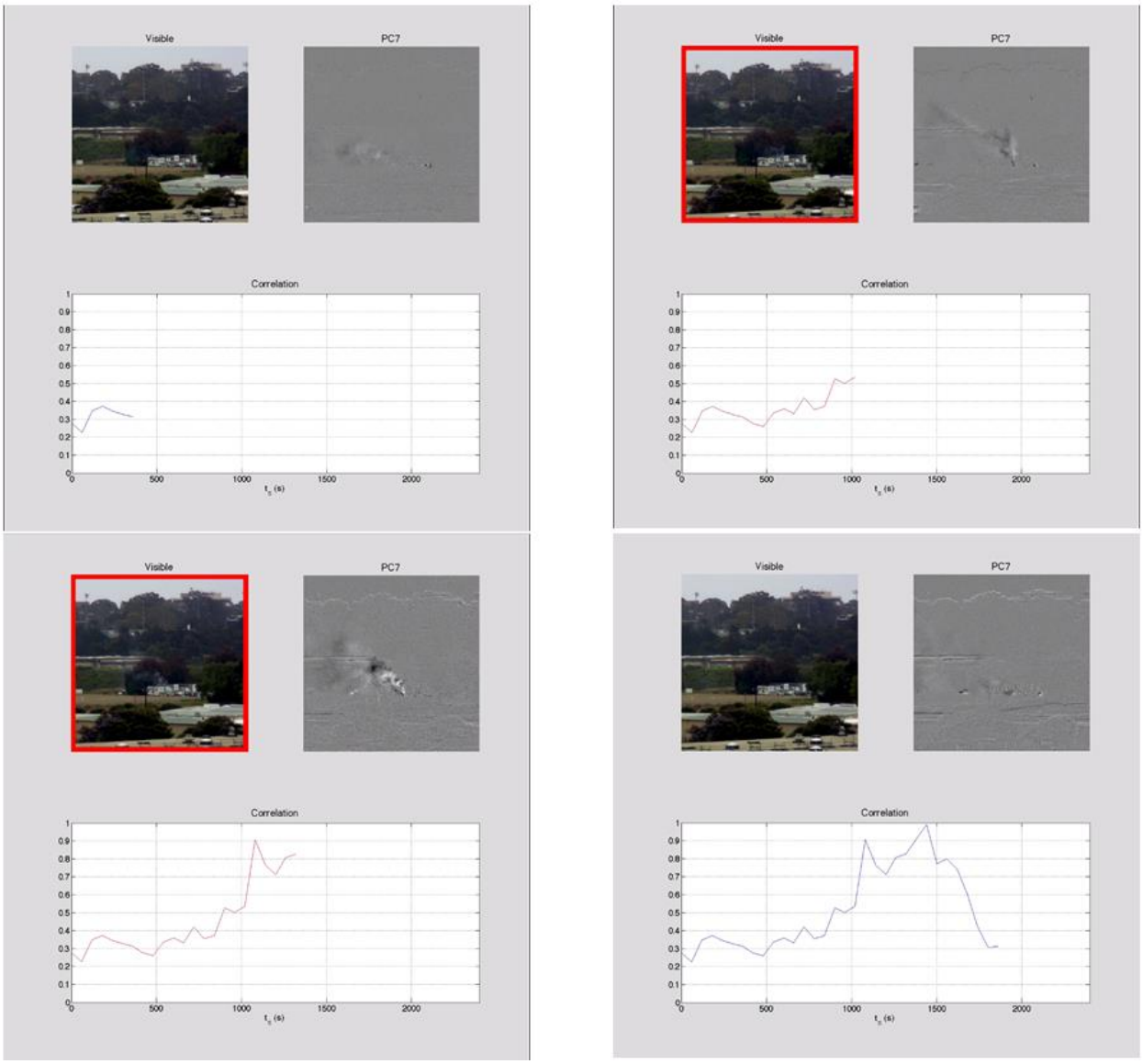

Figure 56 - Composite View of Visible, PC7, and Correlation over time. Source: Davenport

4.1.2 Comparing Heat Plume Detectors

Kohler's PCA of MWIR processes a temporal sequence of MWIR images. MWIR images were pre-processed using the DRMAD filter then processed with PCA. In order to segment a region as heat plume, it had to appear in PC1 as well as another PC image. PC1 is the prominent signal that indicates persistence of heat, and any deeper PC signal in combination with PC1 indicates a positive detection. This method is demonstrated in "EWMA0.05-

0.01_PCA6_auto-th.avi". This method does not detect a large segmented heat plume region, but it is very effective in rejecting noise and false positives.

4.2 Combined Smoke and Heat Plume Detection

An improved fire detection algorithm combines the best methods of smoke plume detection using visible blue spectrum with the best method of heat plume detection using LWIR. Moussa and Garges both demonstrated smoke plume segmentation after PCA with visible blue input images. The main differences are in their pre- and post-processing methods (though both rely mainly on spatial processing). Davenport demonstrated smoke plume segmentation by pre-processing multispectral images with GLCM, then post-processing PCA output using a correlation texture descriptor. This method worked well, but only the visible blue spectrum is a significant contributor to the smoke plume. This method would be improved by removing the other spectra and only using the visible blue spectrum. A single smoke plume algorithm could be designed by combining the principal methods of all three. This smoke plume detector would have stronger sensitivity than all three standalone methods.

In Kohler's method, the prominent signal will be present in PC1 and mostly be contributed by the fire core. The signal in deeper PCs indicates motion of the plume. As a result, this heat plume detector is high in specificity, but not sensitivity (especially compared to smoke plume detection methods). This is due to the smaller spatial footprint of the heat plume compared to smoke plume. Combining the new smoke plume detection algorithm with Kohler's heat plume detection algorithm will improve the specificity of smoke plume detection while increasing the sensitivity of heat plume detection. Stage one of the combined detection is shown in Figure 57, and stage two is shown in Figure 58. The presence of a segmented smoke plume and a

segmented heat plume generates a positive detection. The spatial relationship between the smoke and heat could be used to indicate a confidence level in the detection.

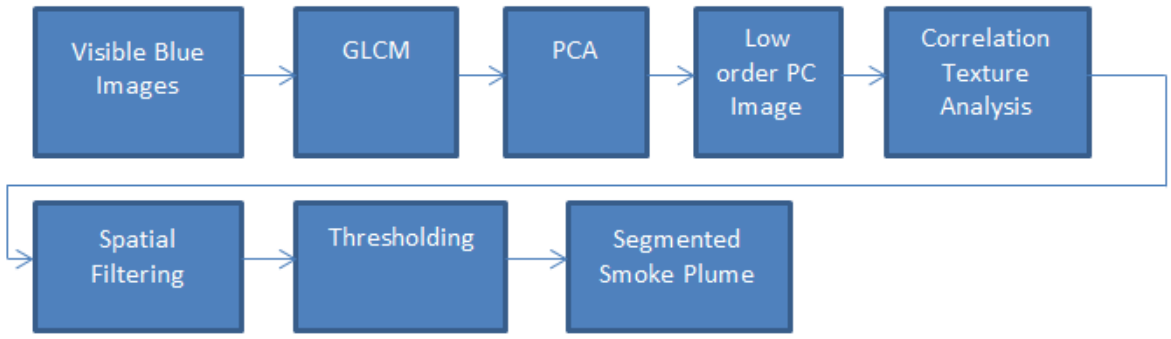

Figure 57 - Smoke Plume Detection

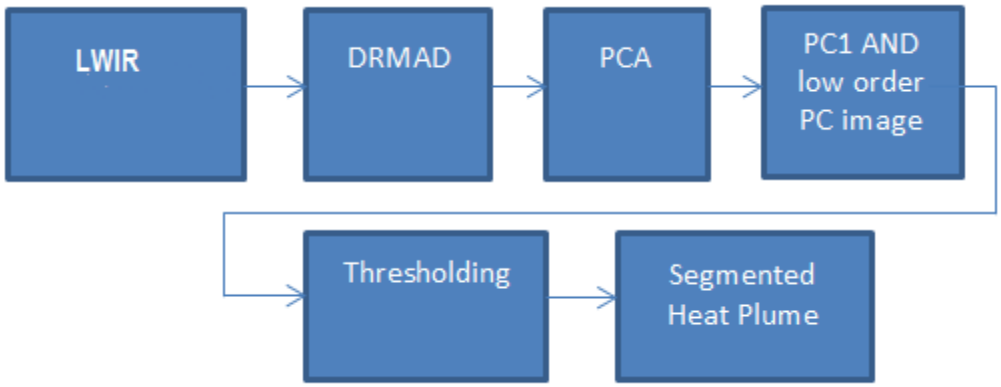

Figure 58 - Heat Plume Detection

4.3 Designing an Early Fire Detection System

4.3.1 Requirements and Expectations

Before a complete EFFD system can be designed, it is important to specify requirements for a detection system. Shall the system detect *all* fires? Shall the system detect fires 24/7? What is a reasonable size of the fire that must be detected? What is a reasonable time to detection?

The previous algorithm designs were held to very high standards in many regards. *The fire source was only the size of a large barbecue and in many cases didn't generate significant heat or smoke to overweigh false positives.* This is a challenging scenario, and it is reasonable to believe that many algorithms will only perform better if a fire were to grow larger. *Fire detection was expected to be calculated too fast.* While faster detection is obviously better, there are tradeoffs between detection time and false positives. Longer time allowed for detection and sampling should reduce false positives.

4.3.2 Fire Detection System Architecture

4.3.2.1 Single Camera System

A single camera system consists of a camera connected to a host system and the internet, see Figure 59. The camera chosen would be a co-located Visible + LWIR camera. The camera has an adjustable sampling rate, and it will stream images via TCP/IP at the rate required by the detection algorithms (defined by the host system). The host system is responsible for storing, processing, classifying the region of interest (ROI) as fire or not, and alerting for human review. The human review is a vague concept, but the idea is to provide human intervention to review positive fire detection and confirm them as true positives or reject them as false positives. The human reviewer will have the ability to interrupt the host system's acquisition and processing thread and override the camera to operate in live camera mode. The live video feed will be streamed to the human reviewer over the internet. The human reviewer can alert fire authorities or reject detection as a false positive. Upon human rejection, the camera returns to its sub-sampled rate and the host system resumes the acquisition and processing thread.

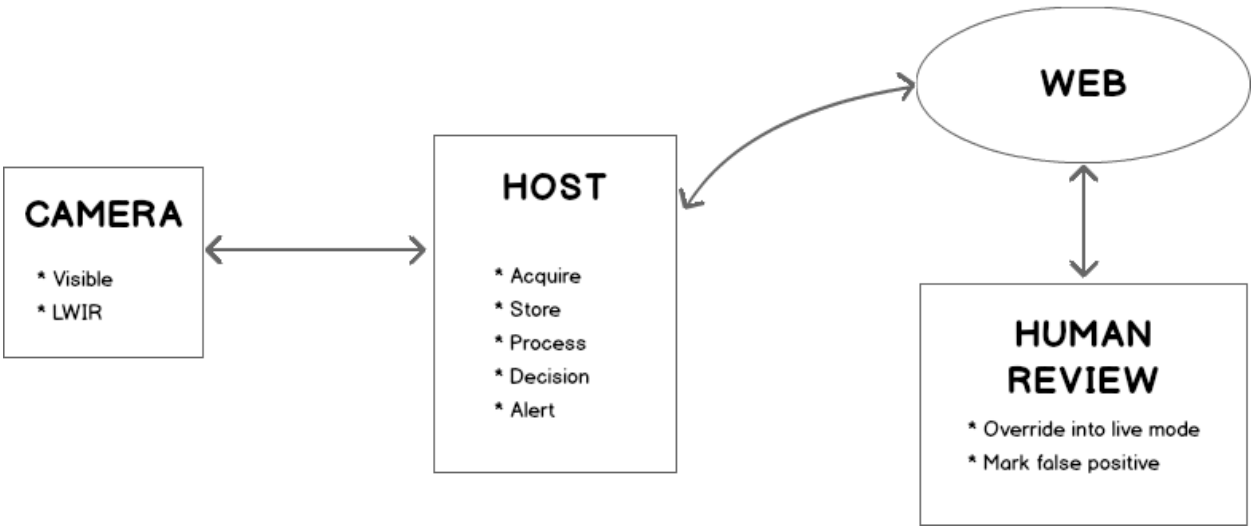

Figure 59 - Block Diagram of Single Camera System

4.3.2.2 Multi-Camera System

A multi-camera system consists of a network of cameras that all feed into the host system for processing, see Figure 60. The host system could be capable of running multiple threads of fire detection algorithms and allocate a single thread for each camera. If the host system detects a possible fire with high confidence, the human reviewer has the same ability to interrupt the detection threads. In addition, the human reviewer could chose to review the live video of all networked cameras until a human classification could be made.

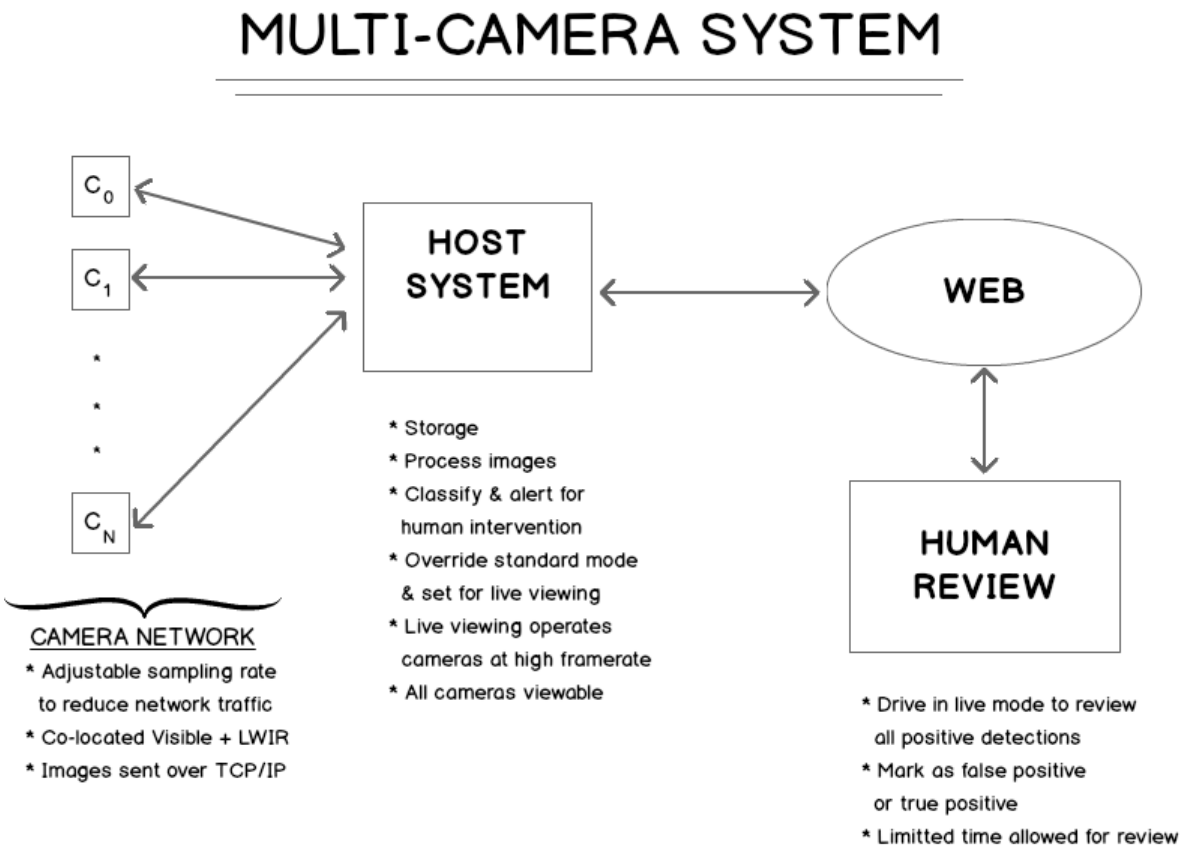

Figure 60 - Block Diagram of Multi-Camera System

4.3.2.3 Single Camera Fire Detection Algorithm

From a high-level perspective, the single camera fire detection algorithm first requires positive detection of a smoke plume via PCA of visible blue images (Moussa + Garges method) and secondly requires positive detection of a heat plume via PCA of LWIR (Kohler method). At this point, the host system can render a classification decision and a confidence level. Since the cameras are most sensitive to smoke plume, it makes sense to run the smoke detection algorithm first. It also makes sense to detect smoke first, since smoke signal is larger than heat signal at the early stages of a fire. If positive smoke plume has been detected, then attempt heat plume

detection for confirmation that a fire scene has been detected. The algorithm and the decision tree for a single camera system are diagramed in Figure 61 and Figure 62.

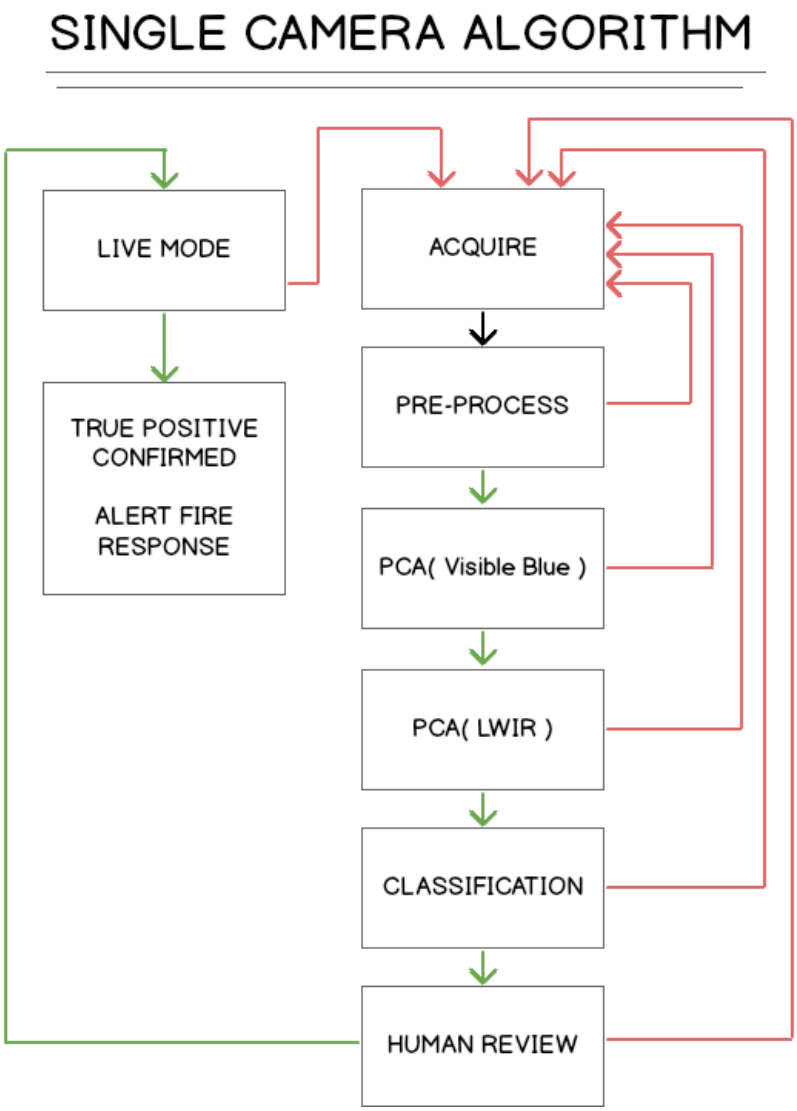

Figure 61 - Algorithm for Single Camera System

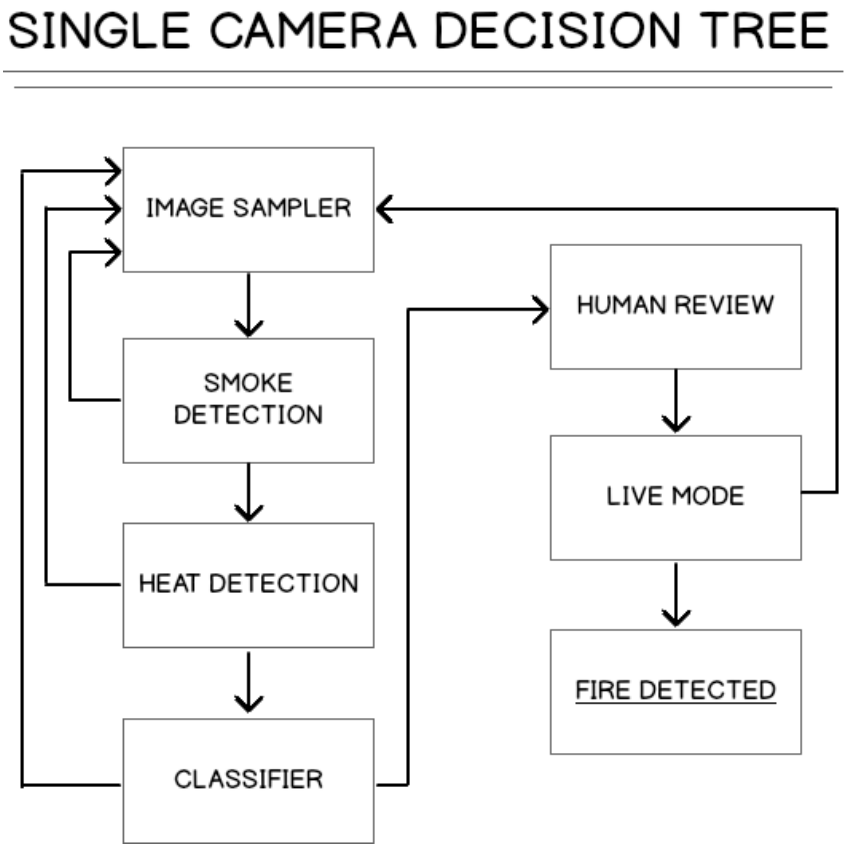

Figure 62 - Decision Tree for Single Camera System

4.3.2.4 Hardware Schematic

A functioning EFFD system cannot consist of mere image processing algorithms. A system architecture must be designed upon which these algorithms can be performed. The EFFD research at Cal Poly up to this point has not included a hardware architecture design. While it may be too early to know the performance requirements of a hardware system, it is not too early to design a functional system architecture that is scalable for processing requirements of the algorithms. A hardware schematic is displayed in Figure 63. The hardware components of the system are described in the bulleted list below.

- Co-located Camera Design

    - Camera1 is Visible
    - Camera2 is LWIR
- Data Acquisition
    - Responsible for capturing data from the camera CCD and transferring to memory
    - DMA transfer minimizes processor load for acquisition
- Storage
    - Capacity depends on the desired storage period
- Processor
    - Embedded processor has power consumption advantages
    - Choice of a traditional architecture lends to easy software development and management
- Motherboard
    - Embedded grade carrier or motherboard
    - Provides the interface between components over buses
        - PCIe
        - SATA
- Networking
    - Wired or wireless designs are possible, depending on proximity to cellular network or internet connection
    - Used for human review of positive detections
    - Monitoring system vitals
- Power
    - Power over Ethernet, Solar, or AC source

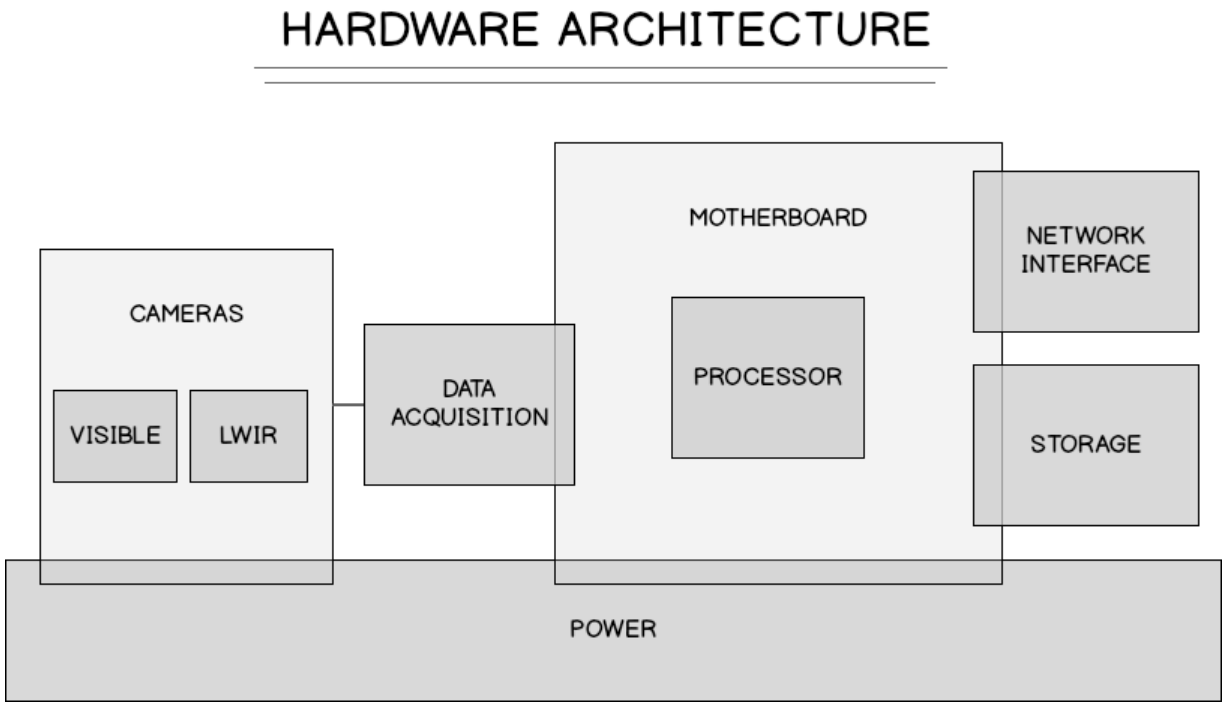

Figure 63 - Hardware Architecture for EFFD System

5 CONCLUSION

5.1 Porting Algorithms from Matlab

A common recommendation from EFFD papers was to port algorithms from Matlab to a true programming language with optimization and embedded capability. All the methods presented were developed in Matlab, and while Matlab is an excellent tool for algorithm development, it is not an optimized language, nor is it a suitable platform for deploying a product. In general, these algorithms must be ported to a compiled language for the possibility of implementing it in an embedded computer.

Matlab Compiler (http://www.mathworks.com/products/compiler/) creates standalone applications as well as callable C/C++ functions for integration with programming languages. This is the easiest way to deploy a Matlab algorithm to an embedded platform, though it is the least optimized approach. A general rule of thumb is that Matlab Compiler provides 10x computation optimization. Perhaps the biggest drawback to Matlab Compiler is that it does not generate readable C/C++ code with comments.

C and C++ are the best languages for deploying an embedded application. C/C++ is the most common language used on embedded processors, whether these are microcontrollers, CPUs, DSPs, or even FPGAs with soft CPUs. While Matlab Compiler is the shortcut, porting to C/C++ manually will provide the most optimization and will allow for the most maintainable software.

OpenCL is a framework language that is best fit for parallel processing on General Purpose Graphical Processing Units (GPGPUs). Applications are broken into parallel kernels that majorly optimize some calculations. Image processing is inherently parallel, and benefits greatly from OpenCL. There is also the indirect advantage of potentially lowered power

consumption. Leveraging a multi-core system can produce the same computation output with a lower clock frequency, which reduces power consumption.

5.2 Open Areas for Research

Some suggestions can be made for future research in EFFD. It would be interesting to run the detection algorithms on additional data. Since the beginning of the Cal Poly EFFD project, many other research groups have collected video data of wildfires that could be training sets for the smoke detection and heat detection algorithms.

Further research can also be more creative and innovative with methods for applying the EFFD algorithms. Cameras are ubiquitous as are networked devices (the Internet of Things). Crowd-sourcing and cloud computing could be very viable platforms for deploying a fire detection algorithm.

5.2.1 More Data

Collaborating with other research groups provides an opportunity to share data. Other research teams have posted videos on YouTube from cameras viewing the birth of a fire. It would be interesting to experiment with EFFD algorithms from these different video sources. This is probably easiest to achieve with algorithms that operate on the visible blue spectrum. Figure 64 shows the formation of a fire from UCSD's High Performance Wireless Research and Education Network (HPWREN) [10].

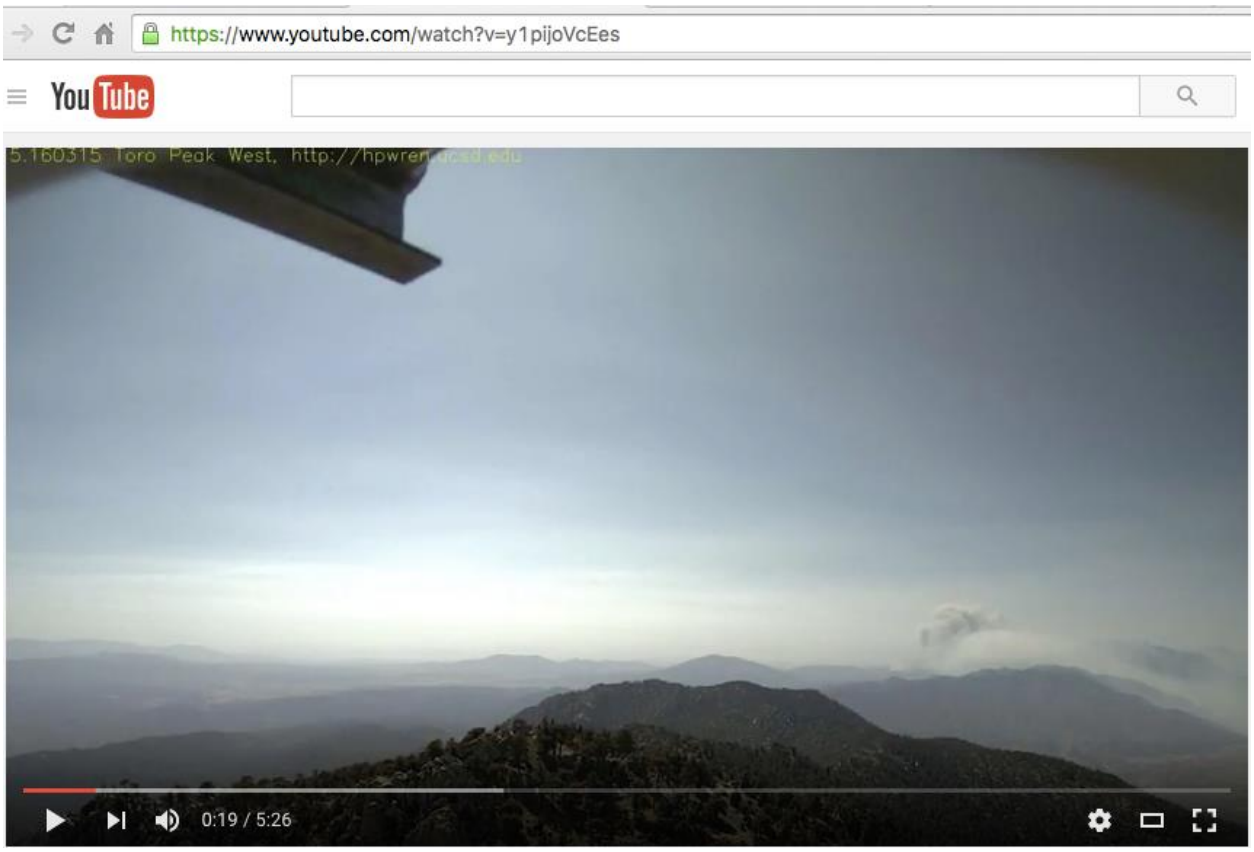

Figure 64 - Riverside County Mountain Fire, July 15, 2013. 2048x1536 images on Toro Peak; camera provided by SDG&E

5.2.2 Crowd and Cloud

A group named Alert-Tahoe at the University of Nevada, Reno is blending old and new schemes by installing a remote, solar powered camera that streams video to a public website, where thousands of volunteers can check on it and manually raise an alarm [11].

Crowd – if human intervention is required, utilizing humans around the world to view and confirm positive detections is possible.

Cloud – if processing is massively intensive, datasets can be transferred to the internet for cloud computation. The major bottleneck in this option is data transmission.

5.2.3 Airplanes

Commercial airline partnerships could have a camera system mounted to survey land for fires during daylight. This obviously provides a very different vantage point as well as a greater viewing distance and a different reflectivity profile caused by the atmosphere.

5.3 Scene Calibration and Parameter Tuning

Calibrating and tuning parameters will be an important and necessary step for any EFFD implementation. For threshold-dependent methods, calibrating a detector would be possible by testing the detection method while generating smoke or heat/fire (man-made) and seeing at what point a true positive can be reached. This can be done at varying distances, heights, backgrounds, etc. to improve the accuracy of the threshold levels.

BIBLIOGRAPHY

[1] National Iteragency Fire Center, May 2016. [Online]. Available: www.nifc.gov.

[2] CCTV America, "YouTube," 27 June 2015. [Online]. Available: https://www.youtube.com/watch?v=6pa3AFibSSw.

[3] J. A. Saghri, R. Radjabi and J. T. Jacobs, "Early forest fire detection using principal component analysis of infrared video," in *Proc. SPIE 8135, Applications of Digital Image Processing XXXIV*, San Dieog, 2011.

[4] G. Moussa, "Early Forest Fire Detection using Texture, Blob Threshold, and Motion Analysis of Principal Components," California Polytechnic State University, San Luis Obispo, 2012.

[5] D. G. Kohler, "Study of Statistical and Computational Intelligence Methods of Detecting Temporal Signature of Forest Fire Heat Plume from Single-band Ground-Based Infrared Video," California Polytechnic State University, San Luis Obispo, 2012.

[6] T. M. Davenport, "Early Forest Fire Detection using Texture Analysis of Principal Components from Multispectral Video," California Polytechnic State University, San Luis Obispo, 2012.

[7] R. A. Aldama, "Early Forest Fire Heat Plume Detection Using Neural Network Classification of Spectral Differences Between Long-Wave and Mid-Wave Infrared Regions," California Polytechnic State University, San Luis Obispo, 2013.

[8] A. J. Boynton, "Early Wildfire Detection Using Temporal Filtering and Multi-Band Infrared Analysis," California Polytechnic State University, San Luis Obispo, 2013.

[9] D. C. Garges, "Early Forest Fire Detection via Principal Component Analysis of Spectral and Temporal Smoke Signature," California Polytechnic State University, San Luis Obispo, 2015.

[10] H.-W. Braun, "YouTube," 18 July 2013. [Online]. Available: https://www.youtube.com/watch?v=y1pijoVcEes.

[11] R. University of Nevada, "AlertTAHOE," [Online]. Available: alerttahoe.seismo.unr.edu.